# Phase diagram of methane and carbon dioxide hydrates computed by Monte Carlo simulations

Waage, Magnus H.; Vlugt, Thijs J.H.; Kjelstrup, Signe

**DOI**
10.1021/acs.jpcb.7b03071

**Publication date**
2017

**Document Version**
Accepted author manuscript

**Published in**
The Journal of Physical Chemistry Part B (Biophysical Chemistry, Biomaterials, Liquids, and Soft Matter)

**Citation (APA)**
Waage, M. H., Vlugt, T. J. H., & Kjelstrup, S. (2017). Phase diagram of methane and carbon dioxide hydrates computed by Monte Carlo simulations. *The Journal of Physical Chemistry Part B (Biophysical Chemistry, Biomaterials, Liquids, and Soft Matter)*, *121*(30), 7336-7350. https://doi.org/10.1021/acs.jpcb.7b03071

Accepted Author's Manuscript

Published in: The journal of Physical Chemistry, Part B.
Vol. 121 (30), pp. 7336-7350.
DOI: 10.1021/acs.jpcb.7b03071

# Phase Diagram of Methane and Carbon Dioxide Hydrates Computed by Monte Carlo Simulations

Magnus H. Waage,[†] Thijs J. H. Vlugt,[‡] and Signe Kjelstrup[*,†,¶]

†Department of Chemistry, Norwegian University of Science and Technology, NTNU, Høgskoleringen 5, 7491-Trondheim, Norway

‡Engineering Thermodynamics,Process & Energy Department, Faculty of Mechanical, Maritime and Materials Engineering, Delft University of Technology, Leeghwaterstraat 39, 2628 CB Delft, The Netherlands

¶PoreLab, Norwegian University of Science and Technology, NTNU, Høgskoleringen 5, 7491-Trondheim, Norway

E-mail: signe.kjelstrup@ntnu.no

Phone: +47 73594179

Abstract

Molecular Monte Carlo simulations are used to compute the three-phase (Hydrate-Liquid water-Gas) equilibrium lines of methane and carbon dioxide hydrates, using the TraPPE model for carbon dioxide, the OPLS-UA model for methane, and the TIP4P/Ice and TIP4P/2005 models for water. The three-phase equilibrium temperatures have been computed for pressures between 50 and 4000 bar via free energy calculations. The computed results behave as expected for methane hydrates, but deviates from direct coexistence Molecular Dynamics studies for carbon dioxide hydrates. At pressures higher than 1000 bar, both methane hydrates and carbon dioxide hydrates dissociate at lower temperatures than expeted from experiments and Molecular Dynamics studies. The dissociation enthalpy is found to be largely independent of water models. The dissociation enthalpy is measured to be 7.6 kJ/mol of water for methane hydrates, and 6.0 kJ/mol of water for carbon dioxide hydrates. We evaluate the effect of systematic errors in the determination of chemical potentials, and show that systematic errors of 0.1 kJ/mol in the chemical potential of water correspond to deviations of 5 K in the three-phase equilibrium temperatures.

# Introduction

Gas hydrates are ice-like structures that form at high pressures when water is in contact with a suitable gas[1]. The crystalline structure is characterized by the formation of several water cages that form around the guest molecules. This, in turn, helps to keep the clathrate structure stable, resulting in hydrates being stable even at temperatures where one would normally expect water to be in liquid form. There are three common hydrate structures:[1] sI, sII and sH. These differ in which cage types they are composed of, and as a result, which guest molecules they hold enclathrated, and which pressures and temperatures they form at.

At the pressures and temperatures we will consider, methane ($CH_4$) and carbon dioxide

($CO_2$) both form sI hydrate[1–4]. In one unit cell of this structure, there are 46 water molecules, which form 2 small (S) cages, defined by 12 pentagonal faces, and 6 large (L) cages, defined by 12 pentagonal and 2 hexagonal faces[1]. At the sea floor, and in permafrost regions, hydrates formed from methane present a sizeable[5] source of energy. The fact that methane and carbon dioxide form the same hydrate structure has led to suggestions that methane can be harvested from hydrates, by replacing it with carbon dioxide[6,7]. A recent review by Chong et al.[8] discusses the potential of harvesting methane from hydrate formations, with a special focus on the $CH_4$-$CO_2$ exchange. To perform such an exchange, it is crucial to properly understand the kinetics and thermodynamics of the exchange process. To determine driving forces, it is necessary to estimate the relative difference in water chemical potential between hydrates of different compositions, as well as the difference in chemical potentials of the guests in gas phase and hydrate phase. In order to avoid an uncontrolled dissociation of methane or carbon dioxide from the resulting hydrate formation, correct estimates of the stability of hydrate formations are needed.

The stability of hydrates is often computed using a combination of equations of state and experimental data. Typically, the fugacity of the guest molecules can be obtained from an equation of state, such as the Peng-Robinson equation of state[9] (PR-EOS), while the filling of the hydrate is described by the van der Waals-Platteeuw[10] (vdWP) model, or one of the more advanced variants[1,11–13]. Combined with the knowledge of a single coexistence point from an experiment, one can estimate the chemical potential difference between liquid water and an empty hydrate at the pressure and temperature of that coexistence point. The chemical potential difference between liquid water and empty hydrate can then be obtained from integration of the residual enthalpies and volumes, along isotherms and isobars.[1] Re-applying the model used to describe the filling of the hydrate, a reasonable estimate of the three-phase equilibrium between hydrate, liquid water and gas phase can be made at all pressures. An unfortunate aspect of

this approach is that the empty hydrate is treated in a manner that depends on the guest in the filled hydrate[1]. For example, the density of an "empty" hydrogen hydrate, is different from the density of an "empty" propane hydrate. In spite of the caveats above, the stability of simple hydrates can be well understood by these approaches[1,14], although care must be taken to obtain accurate results[12].

The kinetics of nucleation remains an important field of study. It was recently reviewed by Warrier et al.[14]. Since the time scales and sizes associated with nucleation are quite small, it is a field of study well suited for molecular simulations[14]. In the study of nucleation kinetics, factors such as the degree of subcooling of the system, diffusivities, and the solubility of guests in water and hydrate are all important in obtaining accurate nucleation rates, as is the chemical potential gradient between the current and final state. In simulations, all of these properties depend on the models used for water and guests[14–18]. In particular, the degree of subcooling in a simulation must be determined using the dissociation temperature and entropy of dissociation of the molecule models, not values obtained from experiments. For this reason, it is important to determine the stability of hydrates directly from molecular simulations[14].

The first direct computation of the phase diagram of hydrates, using molecular models, was performed by Wierzchowski and Monson[19]. Tha work utilized the simple models of water and alkanes developed by Nezbeda et al.[20,21]. Jensen and coworkers[22], expanded on the approach of Wierchowski and Monson and calculated the phase diagram of methane hydrates using TIP4P/Ice[23] and OPLS-UA Methane[24]. The chemical potentials of guests and water molecules were determined in all present phases, by a combination of different molecular Monte Carlo techniques, to be discussed below. By requiring the chemical potential of all phases to be equal, the three-phase equilibrium line was found. Ravipati and Punnathanam, and Pimpalgaonkar et al. used a similar free energy methodology to determine the three-phase line of methane and mixed methane/ethane hydrates[25,26] and other hydrocarbons[27]. This work was done in an

effort to establish a vdWP-like theory with a thermodynamically consistent definition of the empty hydrate. Beyond this, we are not aware of any works that use the method of Wierzchowski and Monson[19]. In particular, we are not familiar with any works studying carbon dioxide in this manner.

More recently, the less involved method of direct coexistence simulations[28] has become popular[15,16,18,29–34] for studying phase coexistence. Several direct coexistence studies have been made studying hydrates[15,16,18,33,34]. In this approach, a system consisting of gas hydrate, liquid water, and free gas molecules is simulated at several different temperatures using Molecular Dynamics (MD) simulations for a long period of time - in one study, simulation times of more than one microsecond were reported[35]. The phase coexistence point is found as the middle point between the highest temperature where the hydrate grows, and the lowest temperature where the hydrate melts.

For methane hydrate, Michalis et al.[16] noted that the results by Jensen et al.[22] appeared to deviate systematically from the results obtained via direct coexistence simulations. Smirnov and Stegailov[34] performed direct-coexistence simulations that agreed with the findings of Jensen et al.[22] Unfortunately, Smirnov and Stegailov[34]'s simulations only considered a system where hydrate was in contact with liquid water saturated with methane to such an extent that methane formed bubbles, rather than a system with all three phases (hydrate, liquid water and methane gas) explicitly present. Additionally, the coexistence-point was evaluated by melting the hydrate in the $NVE$ ensemble, after a "brief" initial equilibration in the $NPT$ ensemble. If the equilibration period was too short, it is unlikely that the methane molecules had time to form a gas phase - as a consequence, the chemical potential of methane will have been highly distorted. Moreover, studying the melting or crystallization in the $NVE$ ensemble is known to strain the solid being simulated[31]. As a consequence, there is no reliable match between direct coexistence simulations and the work by Jensen et al.[22] Clearly, it would be desirable to have correspondence between direct coexistence simulations and free energy-based ones. If such a correspondence cannot be reached, it is necessary to determine why the

methods are divergent. In particular, if the divergence arises due to assumptions made for the direct coexistence simulations, these effects could also appreciably affect MD simulations that study the nucleation of the hydrates, or any other simulations in which two phases are in direct contact. For this purpose, it is useful to provide a detailed analysis of potential systematic errors in the computation of the phase diagrams.

In this work, we have computed the phase diagrams of methane and carbon dioxide hydrates using a free energy based methodology, largely the same as the one used by Jensen et al in Ref.[22]. As noted previously, this technique requires the computation of the chemical potential of water and guests in all phases. This means that a number of sub-problems must be solved, which makes it difficult to keep track of how each specific sub-problem fits into the overall goal. To help remedy this, so that the approach is more accessible, we provide an overview of the techniques used in Fig. 1.

The main goal is to compute the phase diagram of two gas hydrates. Each diagram is represented by the three-phase coexistence line, at which hydrate (h), liquid water (l), and gas (g) phases are in equilibrium with each other. As a condition of thermodynamic equilibrium, the chemical potentials $\mu$ in each phase are equal at constant pressure $P$ and temperature $T$,

$$\begin{aligned} \mu_w^{\mathrm{h}}(x^{\mathrm{h}}, P, T) = \mu_w^{\mathrm{l}}(x^{\mathrm{l}}, P, T) = \mu_w^{\mathrm{g}}(x^{\mathrm{g}}, P, T) \\ \mu_g^{\mathrm{h}}(x^{\mathrm{h}}, P, T) = \mu_g^{\mathrm{l}}(x^{\mathrm{l}}, P, T) = \mu_g^{\mathrm{g}}(x^{\mathrm{g}}, P, T). \end{aligned} \tag{1}$$

Here, $x$ is the composition of each phase. Subscript $w$ denotes water, while $g$ is used for any guest component.

If the solubility of water into the gas phase is negligible, the guest's chemical potential

is only a function of temperature and pressure,

$$\mu_g^{\mathrm{h}}(x^{\mathrm{h}}, P, T) = \mu_g^{\mathrm{l}}(x^{\mathrm{l}}, P, T) = \mu_g^{\mathrm{g}}(P, T), \tag{2}$$

Thus, if we can determine the gas phase chemical potential of the guest component, we can determine the liquid and hydrate phase composition at any pressure and temperature by way of semi grand-canonical Monte Carlo simulations[22,36].

For any pressure, we need to find the temperature at which water in the liquid and water in the hydrate phase have equal chemical potential. For each pressure, we need to compute the water chemical potential difference between the liquid and the hydrate phases at several temperatures in the vicinity of the three-phase line. The three-phase coexistence point is then found as the point where

$$\Delta\mu_w = \mu_w^{\mathrm{l}}(P, T) - \mu_w^{\mathrm{h}}(P, T) = 0. \tag{3}$$

While the individual steps required to determine this point are well established by previous works[22,25,26,36,37], a thorough explanation collected in a single document can be useful. We therefore attempt to cover this in the following sections.

# Method

## System

The molecules used are rigid molecules. The atoms are described by a Lennard-Jones (LJ) potential with a potential depth, $\epsilon_{ij}$, and a range parameter, $\sigma_{ij}$, as well as electrostatic charges, $q_i$. The potential energy of the system is

$$U = U_{\mathrm{LJ}} + U_{\mathrm{el.stat}}, \tag{4}$$

where

$$U_{\mathrm{LJ}} = \sum_{i<j} 4\epsilon_{ij} \left[ \left( \frac{\sigma_{ij}}{r_{ij}} \right)^{12} - \left( \frac{\sigma_{ij}}{r_{ij}} \right)^{6} \right], \tag{5}$$

$$U_{\mathrm{el.stat}} = \sum_{i<j} \frac{q_i q_j}{4\pi\epsilon_0 r_{ij}}, \tag{6}$$

and the sum is taken over all pairs of non-bonded atoms. Lennard-Jones interactions between unlike atoms are treated with modified Lorentz-Berthelot rules[38],

$$\sigma_{ij} = \frac{1}{2}(\sigma_{ii} + \sigma_{jj}), \tag{7}$$

$$\epsilon_{ij} = \chi_{ij}\sqrt{\epsilon_{ii}\epsilon_{jj}}. \tag{8}$$

If the mixing parameter, $\chi_{ij}$ is one, the conventional Lorentz-Berthelot rules are recovered. We have performed simulations using the water models TIP4P/Ice[23] and TIP4P/2005[39], two models that describe the phase diagram of water in a qualitatively accurate manner[23,39]. Of the two, TIP4P/Ice has the closer fit to the experimental phase diagram. Model parameters are shown in table 1. For the guest molecules, we have used TraPPE carbon dioxide[40] and OPLS-UA methane[24]. Both water models have recently been used to study methane[15,16]- and carbon dioxide[17,18] hydrates, using direct coexistence simulations. Studying TIP4P/2005, Docherty et al.[41] showed that a mixing parameter $\chi_{ij} = 1.07$ between the oxygen atom in water and methane was required to correctly estimate the solubility of methane in liquid water. Similar approaches have led to an improved description of carbon dioxide in water[42], and are also known to improve the description of gas hydrates[15,18]. In this work, we have studied the phase diagram as obtained both with and without modified mixing parameters. The choices for mixing parameters are listed together with the guest model parameters in table 2. All simulations were performed with a radial cut-off $r_c = 10$ Å. At this cut-off, Lennard-Jones interactions were truncated and shifted. Appropriate mean field corrections[43] were added. Electrostatic interactions were handled by an Ewald sum-

mation with a relative precision of $10^{-5}$.

To determine the pressures and temperatures where equation (3) holds, we performed classical molecular Monte Carlo simulations. We define the length of these simulations by the number of cycles. In the simulations, a single cycle consisted of on average one attempt to either translate or rotate each molecule. For $NPT$-simulations, there were also two attempts to alter the volume of the simulation box per cycle.

Figure 1, provides an overview of the techniques used to compute $\Delta\mu_w$. We shall now discuss each computational step in detail.

## Pure liquid water

To compute the chemical potential of pure liquid water, $\mu_w^{\mathrm{l}}(P,T)$, we took the rightmost route illustrated in figure 1. We first computed the density of liquid water at the chosen state point by performing $NPT$ simulations that ran for $10^5$ equilibration cycles and $5\times10^5$ production cycles. At this density, we obtained the residual Helmholtz energy of the Lennard-Jones fluid, $F_{\mathrm{LJ}}^{\mathrm{res}}$, from the equation of state of Johnson et al.[44], which we will refer to as LJ-EOS.

Next, the Helmholtz energy of pure liquid water at this density was determined by thermodynamic integration from the Lennard-Jones fluid characterized by the Lennard-Jones parameters of the oxygen atom of the water molecule. The electrostatic interactions of the water molecules were coupled to a parameter $\alpha$ that was varied from 0 to 1. The potential energy of the system under this coupling was $U = U_{\mathrm{LJ}} + \alpha U_{\mathrm{el.stat}}$. The difference in Helmholtz energy between water and Lennard-Jones fluid was computed via thermodynamic integration[43] (TI) at the determined volume,

$$\Delta^{\mathrm{TI}}F_w^{\mathrm{l}} = \int_0^1 \mathrm{d}\alpha \left\langle \frac{\partial U}{\partial \alpha} \right\rangle_{NVT}, \tag{9}$$

where $\langle\cdot\rangle_{NVT}$ denotes an ensemble average in the $NVT$ ensemble. The integral was evaluated using a 16-point gaussian quadrature, where each point corresponded to a simulation of $10^5$ equilibration cycles and $10^6$ production cycles. In this way, we obtained the residual Helmholtz energy of liquid water $F_w^{\mathrm{l,res}} = F_{\mathrm{LJ}}^{\mathrm{l,res}} + \Delta^{\mathrm{TI}} F_w^{\mathrm{l}}$. Finally, the residual chemical potential of liquid water at the chosen pressure and temperature was obtained as

$$\begin{aligned}\mu_w^{\mathrm{l,res}}(P,T) =& \frac{G(P,T) - G^{\mathrm{id}}(P,T)}{N_w} = \frac{F(V(P),T) - F^{\mathrm{id}}(V^{id}(P),T) + P(V - V^{\mathrm{id}})}{N_w} \\ =& \frac{F_w^{\mathrm{l,res}}(V(P),T) + P(V - V^{\mathrm{id}})}{N_w} - RT\ln(\frac{V}{V^{\mathrm{id}}}),\end{aligned} \tag{10}$$

where $V^{\mathrm{id}} \equiv V^{\mathrm{id}}(P,T)$ is the volume of the ideal gas at the considered pressure and temperature, and $R$ is the universal gas constant.

## Empty hydrate structure

We now turn our attention to the empty hydrate, which we shall refer to by $\mathrm{h}_0$. The chemical potential of water in an empty hydrate structure was found by following the leftmost path in figure 1. First, a $2 \times 2 \times 2$ unit cell sI hydrate structure was constructed. Oxygen atoms in the hydrate structure were placed according to X-ray data by McMullan and Jeffrey[45], while the protons were configured according to data by Takeuchi et al.[46] We determined the density of the empty hydrate structure using $NPT$ ensemble simulations. At the determined density, we determined the residual Helmholtz energy of an Einstein crystal with rotations[47]. In this Einstein crystal, the molecules are bound to their "ideal" positions $r_i^0$ and orientations by spring potentials,

$$U_{\mathrm{E}} = \lambda_T(\mathbf{r_i} - \mathbf{r_i^0})^2 + \lambda_R\left[\sin^2\phi_a + \left(\frac{\phi_b}{\pi}\right)^2\right]. \tag{11}$$

Here, $\mathbf{r_i}$ is the current position of the molecule's center of mass, while $\phi_a$ and $\phi_b$ represent the rotation away from the ideal orientation, defined as in Ref. [47]. For the spring constants, we used values of $\frac{\lambda_T}{RT\text{Å}^2} = \frac{\lambda_R}{RT} = 25000$. The residual Helmholtz energy of such an Einstein crystal is[47–50]

$$\frac{F^{\mathrm{E,res}}}{RT} = -\ln(N^{3/2}(\frac{RT\pi}{\lambda_T})^{\frac{3}{2}(N-1)}) - N\ln(J(\frac{\lambda_R}{RT})) - \ln(\frac{V}{N}) + N(\ln(\frac{V}{N})+1) + \ln N + \frac{\ln \pi}{2}, \tag{12}$$

in which the rotational contribution is[47,50]

$$J(\frac{\lambda_R}{RT}) = \ln\left[\int_0^1 \mathrm{d}x \exp(\frac{\lambda_R}{RT}(1-x)^2) \int_0^1 \mathrm{d}y \exp(\frac{\lambda_R}{RT}(-y)^2)\right]. \tag{13}$$

For the thermodynamic integration, we used a coupling parameter $\alpha$ to construct a potential where the Einstein crystal potential was switched off smoothly, while the "real" interactions were switched on, $U = \alpha U_{\mathrm{E}} + (1-\alpha)U_{\mathrm{real}}$. This approach differs slightly from the approach in Refs.[22,36], where the interactions were turned on discontinuously using an umbrella simulation. While that would be necessary for a hard sphere system, the water molecules are characterized by continuous interactions, so a smooth integral from Einstein crystal to "real" crystal is allowed. When $\alpha$ approaches 0, the integrand increases rapidly, resulting in a potential numerical instability. As described in Ref. [48], we therefore performed the integration in logarithmic space,

$$\Delta^{\mathrm{TI}} F^{\mathrm{h_0}} = \int_{\ln(c)}^{\ln(1+c)} (\alpha + c) \left\langle \frac{\mathrm{d}U}{\mathrm{d}\alpha} \right\rangle \mathrm{d}\ln(\alpha + c), \tag{14}$$

using an integration constant $c = 10^{-5}$, for which the integral was numerically stable. Again, the thermodynamic integrand was evaluated using a 16-point gaussian quadrature. The simulations in this section were performed for $10^5$ equilibration cycles and $5\times10^5$ production cycles. Having performed the thermodynamic integration, the empty

hydrate Helmholtz energy was determined by

$$F^{\mathrm{h_0,res}} = F^{\mathrm{E,res}} + \Delta^{\mathrm{TI}} F^{\mathrm{h_0}} - TS^{\mathrm{res}}, \tag{15}$$

where we used the Nagle estimate for the residual entropy of ice[51], $S^{\mathrm{res}} = 0.410NR$. Finally transitioning from constant volume to constant pressure, the residual chemical potential was found in a similar manner as in equation (10), as

$$\mu_w^{\mathrm{h_0,res}}(P,T) = \frac{F_w^{\mathrm{h_0,res}}(V(P),T) + P(V - V^{\mathrm{id}})}{N_w} - RT\ln(\frac{V}{V^{\mathrm{id}}}). \tag{16}$$

## Chemical potential of guests

To compute the guest chemical potentials in the gas phase, $\mu_g^{\mathrm{g}}(P,T)$, we followed the central path of figure 1. The steps involved in this procedure are in principle the same as those described for pure liquid water, although methane is described as a single Lennard-Jones interaction site, and thus does not require any thermodynamic integration. We compared these chemical potentials to ones obtained from the PR-EOS[9], which, if it can be used, would provide the fugacity of gases in a more convenient matter. This would be useful for the study of mixed-component hydrates. The input parameters used in the PR-EOS are listed in table 3.

## Test for self-consistency

To ascertain the correctness of the computed chemical potentials of liquid water and the empty hydrate, we computed the chemical potential directly, as described above, but also by integration along isotherms and isobars[22], as follows

$$\frac{\mu_w^{\mathrm{res}}(P_2,T_2)}{RT_2} = \frac{\mu_w^{\mathrm{res}}(P_1,T_1)}{RT_1} + \int_{P_1}^{P_2} \frac{V(P,T_1) - V^{\mathrm{id}}(P,T_1)}{N_w}\mathrm{d}P - \int_{T_1}^{T_2} \frac{H^{\mathrm{res}}(P_2,T)}{RT^2}\mathrm{d}T, \tag{17}$$

This was done for all temperatures and pressures. The chemical potentials obtained in this manner were consistently within ±0.001 kJ/mol of those obtained from thermodynamic integration at each pressure and temperature.

## Filling the hydrate structure

Finally, we considered filling the hydrate structure. The chemical potential of water in a filled hydrate was related to that of the empty hydrate[36], by integrating the Gibbs-Duhem equation

$$\Delta\mu_w^{\mathrm{h,res}} = \mu_w^{\mathrm{h,res}} - \mu_w^{\mathrm{h_0,res}} = -\frac{1}{N_w}\int_{-\infty}^{\mu_g} N_g \mathrm{d}\mu_g', \tag{18}$$

where the upper bound is the chemical potential of the guest component in pure guest phase, which we found earlier. The lower bound corresponds to the chemical potential of a guest in a completely empty hydrate. To compute the integrand for any given pressure and temperature, we performed a set of semi grand-canonical simulations of the hydrate system. In each simulation, the pressure, temperature, total number of water molecules, and chemical potential of guest species were kept constant, meaning that the number of guest molecules was allowed to fluctuate. The sI hydrate is made up of 6 large cages and 2 small cages per unit cell. In other words, there are $\theta^L = 6/46$ and $\theta^S = 2/46$ large and small cages per water molecule. We explicitly computed the fractional occupancy of each cage $x_{\mathrm{occ}}^{\mathrm{L/S}}$. To compute the fractional occupancy of cages, we computed the distance between each guest molecule, and the center of mass of each cage, as determined by the positions of the water molecules that constitute the cage. While water molecules are very mobile during simulations, we did not observe any water molecules swapping positions. Thus, the water molecules could be assigned to cages at the beginning of the simulations. The radius used to determine which cage a guest molecule occupied was chosen conservatively to 3.3 Å. This radius guaranteed that a guest molecule would never be assigned to two cages at the same time. It did also result

in some guests not being assigned to cages. In the most extreme cases, this resulted in a relative inaccuracy of less than $10^{-5}$ in the estimated fractional occupancy. If desired, the accuracy could be improved by using different radii for large and small cages. We fitted the measured occupancies to Langmuir isotherms,

$$x_{\mathrm{occ}}^{\mathrm{L/S}} = \frac{C_g^{L/S} f_{\mathrm{g}}}{1 + C_g^{L/S} f_{\mathrm{g}}}, \tag{19}$$

where $C_g^{L/S}$ are the Langmuir constants for the large and small cages and guest $g$. The fugacity, $f$, is related to the residual chemical potential of the guest as $f = P\exp(\mu_g^{\mathrm{res}}/RT)$. Since $\frac{N_g}{N_w} = x^{\mathrm{L}}\theta^{\mathrm{L}} + x^{\mathrm{S}}\theta^{\mathrm{S}}$, this fit allows us to solve equation (18) analytically,

$$\frac{\Delta\mu_w^{\mathrm{filling}}}{RT} = \theta^L \ln(C_g^L f_g + 1) + \theta^S \ln(C_g^S f_g + 1). \tag{20}$$

Due to guest-guest interactions, and the deformability of the water cages, such a fit cannot be completely precise[36]. As was the case with liquid water solubility, it is necessary to estimate to which extent the error due to this assumption affects the computed phase diagram. To obtain the isotherms, we performed 64 simulations for each temperature/pressure combination considered, varying chemical potentials in such a way as to evenly cover the adsorption isotherm of the guest components. Each simulation lasted $10^5$ equilibration cycles and $3 \times 10^5$ production cycles. We utilized the CFCMC[52] methodology with a bias obtained using the Wang-Landau method[53] to improve the efficiency of the simulations. In this approach, a fractional molecule is used to improve the rate of insertion and deletion of guest molecules. The fractional molecule acts with interactions that are modified by a fractional parameter $\lambda_f$, which alters electrostatic interactions[52],

$$q_i^{\mathrm{frac}} = \lambda_f^5 q_i \tag{21}$$

and Lennard-Jones interactions[52],

$$U_{\mathrm{LJ,frac}} = \lambda_f 4\epsilon_{ij}\left[\left(\left(\frac{r_{ij}}{\sigma_{ij}}\right)^6 - \zeta_f(1-\lambda_f)^2\right)^{-2} - \left(\left(\frac{r_{ij}}{\sigma_{ij}}\right)^6 - \zeta_f(1-\lambda_f)^2\right)^{-1}\right], \quad (22)$$

where $\zeta_f$, in this case was chosen as 0.5. The CFCMC methodology is described in further detail in the following references[52,54–56]. In the CFCMC simulations, 100 attempts to change the fractional parameter of the fractional molecules were made per cycle, in addition to the normal moves named previously. Every cycle, we sampled the total number of (non-fractional[55]) molecules present in the system. We explicitly counted how many small and large cages were occupied by non-fractional molecules.

Computing the adsorption isotherms at each combination of pressure and temperature is a computatinally expensive procedure. Pimpalgaonkar et al.[25] demonstrated that the phase diagram can be obtained in a cheaper manner, by performing a full evaluation only at a chosen reference state, and otherwise computing occupancies corresponding to the gas fugacities obtained at the pressure and temperature. Care should still be taken to compute the full adsorption curve at intervals, to root out any systematic deviations.

By completing this step, we found the chemical potential of water in a hydrate that is filled with guests according to the guest chemical potential. Thus, we computed $\Delta\mu_w(P,T)$. Using linear interpolation, we determined the temperatures at which $\Delta\mu_w(P,T) = 0$, and obtained the three-phase equilibrium line.

## Solubility of guests in liquid water

At the conditions considered, both methane and carbon dioxide are sparingly soluble in water. The mole fraction $x_{\mathrm{g}}$ of guests dissolved in water was therefore determined,

using the Krichevsky-Kasarnovsky equation[57,58],

$$\lim_{x_{\mathrm{g}} \to 0} \frac{f}{x} = H_{\mathrm{gw}} e^{\frac{v_{\mathrm{g}}}{RT}(P - P^0)}, \tag{23}$$

where $H_{\mathrm{gw}}$ is the Henry constant of the guest mixed in water, $v_{\mathrm{g}}$ is the partial molar volume of the guest, and $P^0$ is the reference pressure at which $H_{\mathrm{gw}}$ was defined. The value of $H_{\mathrm{gw}}$ was obtained from the NIST database[59,60]. For partial molar volumes, we used values from Moore et al.[61], which were obtained at 298.15 K. We neglected the temperature and pressure dependence of the partial molar volume. For methane, we used the correlation presented in ref[62] to estimate the error in the solubility due to neglecting the temperature dependence of the partial molar volume. For pressures lower than 1000 bar, it is less than 10% for a temperature difference of 40 K. At higher pressures, the error increases, but at the three-phase equilibrium points, it remains less than 20%. We expect the error due to neglecting the pressure-dependence to be similar.[63,64] The solubility of $CO_2$ computed in this manner is high enough that it can appreciably affect the computed three-phase equilibrium temperature. For this reason, we explicitly computed the solubility by performing CFCMC simulations for $10^5$ equilibration cycles and $5 \cdot 10^6$ production cycles, using a system of 400 water molecules. For methane, no such additional simulation was performed.

By obtaining $x_{\mathrm{g}}$, the corresponding change in the residual chemical potential of liquid water can be expressed as[22]

$$\Delta\mu_w^{\mathrm{l,res}}(P,T) = RT \ln(1 - x_{\mathrm{g}}). \tag{24}$$

# Results and discussion

## Guest Chemical Potential

In figure 2, we have plotted the difference in the guests' chemical potentials as calculated from simulations or from the PR-EOS[9] as a function of pressure at 280 K. For carbon dioxide, the PR-EOS computes an residual chemical potential as much as 1.0 kJ/mol higher than that obtained from simulations. The difference appears to be strongly pressure dependent. The maximal difference appears to be between 50 and 100 bar, which is reasonable as the critical pressure of TraPPE carbon dioxide is 77.7 bar[65]. The deviation did not seem to vary much with temperature. Clearly, the PR-EOS is unsuitable near the critical point of the gas, an unsurprising result. However, the deviation is noticeable also at higher pressures, remaining as high as 0.2 kJ/mol at a pressure of 2000 bar. From equation (18), we estimate that a systematic error in the $CO_2$ chemical potential of 0.5 kJ/mol corresponds to an error in the water chemical potential of 0.09 kJ/mol. For methane, the difference between the PR-EOS and the chemical potential obtained from the LJ-EOS[44] shows a less clear dependence on pressure. Still, the PR-EOS can yield a chemical potential that is as much as 0.34 kJ/mol lower than the one obtained from the LJ-EOS.

## Adsorption isotherms

Figures 3 and 4 present representative adsorption isotherms for methane and carbon dioxide. We show adsorption isotherms for two pressures, 50 and 4000 bar, which were the end points of the pressures studied in this work (marked by black squares). It is immediately clear that carbon dioxide is a two-site isotherm. For methane, this is also so, although the difference between the small and large cages is less pronounced than for carbon dioxide. The adsorption isotherms are shifted slightly to lower occupancy/ higher fugacity as the applied pressure increases, reflecting that there is a compression

of the hydrate structure. In the pressure range considered, this can best be seen in the adsorption isotherm that reflects filling of the small cages - the large cages remain large enough so that the decrease in cage volume is negligible. For $CO_2$, the shift is large enough to observe a difference when the isotherm at 50 bar is compared to the isotherm at 4000 bar. Methane has an adsorption isotherm for small cages that is noticeably shifted, but the change is so small that there is no significant effect on the total adsorption isotherm. Regardless, it is expected that a stronger shift will occur at even higher pressures.

We have found that the Langmuir isotherms of equation (19) fit reasonably well. There is, however, a noticeable deviation at lower occupancies, as well as a smaller, opposite deviation at higher occupancies. A deviation is expected, as the guests interact with each other, and also cause deformations to the cage structure, implying that the adsorption energies vary with occupancy. In the past, Wierchowski and Monson[36] studied the effect of neglecting these phenomena on the accuracy of the van der Waals-Platteuw model. Those authors found that the effect due to ignoring the deformability of water cages led to errors in the adsorption isotherm, that roughly cancelled those that arose from ignoring guest-guest interactions. The good fit of the Langmuir isotherms might be a consequence of this fact. In Fig. 5, we have computed the difference between using the analytical fit and a trapezoidal integration of the simulated results in the evaluation of equation (18). For both methane and carbon dioxide, the error was less than 0.03 kJ/mol, for all chemical potentials considered, with a maximal error occuring when the hydrate is half loaded. We verified that this was the case for all temperatures and pressures considered, but have only presented the error for a single temperature and pressure for the sake of clarity. The error was similar for both methane and carbon dioxide. It is plausible that it will vary for different guest molecules.

Ravipati and Punnathanam[27] calculated pressure-dependent Langmuir constants for four hydrocarbons in TIP4P/Ice, in a vdwP-like theory meant to treat the empty hydrate in a more rigorous manner, obtaining good agreement with experiment for

methane up to 1000 bar. As the adsorption isotherm for methane appears to be only weakly pressure dependent up to this pressure, it would be interesting to see how well their method treats the $CO_2$-hydrate. The phase diagram of this hydrate is more strongly pressure dependent, and has been challenging to model with other vdwP-based approaches[12,13].

## Liquid phase solubilities

As a first effort, the solubility of guests in liquid water was estimated using equation (23) in combination with experimental values for the Henry constants[59,60] and the partial molar volumes of methane[62] and carbon dioxide[66]. For methane, the mole fraction obtained from equation equation (23) is, at all points considered, lower than 0.007. This corresponds to an estimated effect on the liquid water chemical potential between 0.003-0.02 kJ/mol. For carbon dioxide, the estimated liquid phase mole fraction varied between 0.02 and 0.03. From equation (24), this implies a contribution to the liquid water chemical potential of 0.05-0.09 kJ/mol. In the following section, we analyze the effect of systematic errors on the determination of the three-phase equilibrium points. For methane, the estimated solubility in water was low enough that it can be neglected. For carbon dioxide, however, the solubility is not negligible. Therefore, we also calculated the solubility of $CO_2$ explicitly with CFCMC simulations. The solubilities measured in this manner are presented in tables 12-15. In general, the solubilities deviated from the solubilities obtained via (23) by less than 25%, when the Lennard-Jones interactions were modified by $\chi_{ij}$. The simulated solubilities appeared to be more strongly pressure dependent than those obtained via equation (23) - this could be due to the approximate nature of the input we used for the Krichevsky-Kasarnovsky equation. For TIP4P/Ice, we never measured a carbon dioxide mole fraction higher than 0.045 in the pressure and temperature ranges considered. Further, we obtained a maximal solubility at 2000 bar, with a decrease in mole fraction for the simulations at

4000 bar. This is significantly different from Costandy et al.[18], who reported a mole fraction as high as $\sim 0.07$ at 4000 bar and 293.6 K, with the solubility consistently increasing with higher pressure. Indeed, our observed solubilities are consistently lower than those reported by Costandy et al. Qualitatively, our observed solubilities fit with what Costandy et al.[18] report up to 2000 bar. After this, the measured solubilities diverge sharply. Unfortunately, the correlation of Duan et al[67], which Costandy et al. have compared their results to, is unapplicable at pressures above 2000 bar. We have not been able to find other works studying the solubility of $CO_2$ at these high pressures. While our observed behavior fits with that of the Krichevsky-Kasarnovsky equation, it is plausible that our application of this equation is inaccurate at 4000 bar, as was discussed previously. Regardless, we have faith that our measured solubilities are accurate. For simulations with unmodified Lennard-Jones interactions, the measured mole fractions were lower than for those with modified Lennard-Jones interactions by approximately 0.01.

## Dissociation entropy and a discussion on systematic errors

In figure 8, we show how $\Delta\mu_{\mathrm{w}}$, as defined in equation (8), varies with temperature. As can be seen, a linear fit is appropriate, even in the relatively wide temperature range that has been considered. The slope of the curve corresponds to minus the entropy of dissociation, $\Delta_d S$. The value of $\Delta_d S$ appeared to be only weakly dependent on the which guest was enclathrated. The estimated values were between 21 and 30 J/K mol of water, and are reported in tables 6-11. The values for $\Delta_d S$ informs us of the sensitivity of the three-phase equilibrium points to systematic errors in the chemical potential calculations. A systematic error of 0.1 kJ/mol corresponds to a $\sim 5$ K displacement of the three-phase line, as illustrated in figure 8. To use the analytical expression for the adsorption isotherms will, at most, cause a 1.5 K shift of the phase line. For carbon dioxide, a more dramatic shift would be obtained from using the PR-EOS to compute

fugacities at the lower pressures - at 50 bar, that would cause a shift of nearly 10 K!

A further shift can be caused by the finite-size effects of the empty hydrate. Moustafa et al.[68] studied the effect of finite size on estimates of the free energies of empty clathrate hydrates. As is the case with monatomic crystals[49], Moustafa et al.[68] found that the leading-order finite-size contribution scales as $-RT(\ln N)/N$. For a $2 \times 2 \times 2$ unit cell sI hydrate at the temperature ranges we have considered, this implies a contribution of $0.03 - 0.04$ kJ/mol. Of the direct coexistence works we have studied, none exceed dimensions of $N_x \times 2 \times 2$, where $N_x$ varies between 2 for the initial hydrate seed, to 6 for systems where all the water is consumed. For those systems, we would expect a finite size correction of roughly 0.01 kJ/mol, implying that there could be a systematic difference of $0.02 - 0.03$ kJ/mol relative to those works, which is of the same magnitude as the error caused by fitting a Langmuir isotherm to the adsorption isotherm.

## Dissociation enthalpy

In tables 6-11, we report the entropies and enthalpies of dissociation at the three-phase coexistence temperatures. The entropies and enthalpies show no clear dependence on pressure or water model. For the methane hydrate, the enthalpy of disscociation varies between 7.0 and 8.1 kJ/mol of water. The average value measured is 7.6 kJ/mol. Using a high pressure differential scanning calorimeter, Gupta et al.[69] reported an enthalpy of dissociation of 9.1 kJ/mol of water. The values we report are $10 - 25$ % lower than this, something which is consistent with results for the melting enthalpy of ice[39]. In their simulation of the methane hydrate with TIP4P/Ice, Jensen et al.[22] reported a dissociation enthalpy of 9.2 kJ/mol of water at 25 bar, which would appear to be in very good agreement with experimental values. However, Jensen et al. calculated the dissociation enthalpy using the Clausius-Clapeyron equation. Experimentally, it is known that the Clausius-Clapeyron equation mispredicts the dissociation enthalpy for higher

pressures[69], since it neglects the volume difference between liquid water and hydrate. We believe that their seemingly accurate dissociation enthalpy is an artifact that is due to the inaccuracy of the Clausius-Clapeyron equation.

For carbon dioxide, we find somewhat lower values, $\Delta_d H$ lies between 5.3 and 6.5 kJ/mol of water, with an average of 6.0 kJ/mol, 1.6 kJ/mol less than for methane hydrate. Using the Clapeyron equation (not to be mistaken for the Clausius-Clapeyron equation), Anderson[70] reported a value between 9.63 and 10.3 kJ/mol of water - an increase of 0.5 - 1.2 kJ/mol compared to methane hydrates. This is the opposite development from our simulated results, so the deviation between our values and experimental results increases to $\sim$ 40% when going from methane to carbon dioxide hydrates. This is a relatively large difference from experimental values. As discussed for methane hydrate, we can expect the water model alone to contribute a deviation of as much as 20%. The remaining deviation is necessarily due to an inaccurate description of either the water-$CO_2$ interactions, or the description of pure carbon dioxide.

## Phase diagrams

In figures 9 and 10, we present the phase diagram of methane hydrate, as computed by Monte Carlo simulations in this work, together with values collected from other simulations[15,16,26] and experiments[2]. For both TIP4P/2005 and TIP4P/Ice, our work results in a phase diagram closely corresponding to the direct coexistence simulations of Michalis et al.[16] and Conde and Vega.[15] We note that there is still a systematic deviation of roughly 3 K relative to Michalis et. al.[16] In their direct coexistence simulations, tail corrections to the Lennard-Jones interactions were not included, due to the non-isotropy of the system. In our simulations, these corrections are included, as each simulation box only considers a single phase. It is possible that this last systematic deviation is due to this difference. Regardless, the deviation is far smaller than the results presented by Jensen et al.[22]

At high pressures, the phase diagram of the methane hydrate appreciably deviates from the experimental data. It is possible that this is an indication that retrograde behavior occurs at an earlier pressure than what is expected from experiment[71]. Smirnov and Stegailov[34] found a closer match with experimental values near 5000 bar, but as discussed in the introduction, that work had methodological issues that make the reported results unreliable. It is not unexpected to see mild deviations from the experimental phase diagram; such deviations also exist for the other ices[37].

In figures 11 and 12, we show the phase diagram for carbon dioxide hydrate. For low pressures, the results appear to be well behaved with respect to experimental data[3,4], as well as direct coexistence simulations[17,18]. As pressure increases, there appears to be a small qualitative deviation from literature and direct coexistence simulations. The coexistence temperature is steadily shifted towards lower temperatures, compared to what could be expected from experimental results. It is not immediately clear where this deviation arises. We can, however, exclude the computation of the chemical potentials of pure liquid water and empty hydrate, as those same values were used when computing the phase diagram for methane hydrate, which seems to be well behaved for pressures up to 1000 bar.

Previously, we discussed the solubility of carbon dioxide, as computed from CFCMC simulations, which is listed in tables 14-15. When pressure increases, this measured solubility is lower than the one measured by Costandy et al.[18]. By itself, this reduced solubility would imply that the hydrate is more stable at higher pressures, implying that we should expect the opposite deviation than what we observe. But it is possible that this reduced solubility is caused by a difference in the fugacity of carbon dioxide at high pressures. In our simulations, such a difference would more strongly affect the chemical potential of water in the hydrate phase, which would explain the qualitatively different behavior. It is not immediately clear why such a difference occurs. Ultimately, we suspect three possible culprits. First, our simulations are performed with a slightly

shorter radial cut-off, 10 Å, compared to the 11 Å of Costandy et al[18]. Next, Costandy et al. had to perform their simulations without accounting for analytical tail corrections, since the direct phase coexistence simulations are non-isotropic and non-homogeneous[16]. Studying methane, Michalis et al.[16] found that discarding the tail corrections caused a change in gas phase density of 5 - 10%. While they did not find that this amount affected the stability of the methane hydrate, it is plausible that it could affect the carbon dioxide phase diagram, especially since the carbon dioxide simulations were performed at a higher pressures, where density differences have a stronger effect on the Gibbs energy. Additionally, the simulations with carbon dioxide are performed at conditions that are close to the critical point. This could accentuate any effects from different treatments of the analytic tail corrections, a phenomenon which is well known[43]. A final possible reason for the observed differences, is the use of different barostats. The barostat employed in the direct coexistence simulation is anisotropic, so as to avoid a shear strain between distinct phases. It is possible that this hinders the deformation of the hydrate cage, which would improve the likelihood of carbon dioxide being enclathrated, thus improving the stability of the hydrate structure.

Of these reasons, the first seems to put undue weight on the choice of cut-off radius, while the third and fourth fail to explain the difference in solubility in liquid phase. Thus, we propose that the elimination of tail corrections in the direct coexistence simulations is the reason for the deviation between those simulations and our own. If so, direct coexistence simulations that employ a longer cut-off range should deviate from the simulation of Costandy et al.[18], and converge towards the results from our simulations. It might also be helpful if the direct coexistence simulations are performed with the inclusion of long-term corrections that have been developed for multi-phase systems[72,73]. It is however, also possible that the discrepancy between the present work and the direct coexistence simulations is due to inherent differences between the two methodologies. A similar discrepancy is reported for the study of the solubility of sodium chloride[74,75] - to our knowledge, this discrepancy has yet to be resolved.

For all considered pressures, the solubility of carbon dioxide in water is lower than experimental values[67], as well as those reported by Costandy et al[18]. The deviation increases with increasing pressure. The same is true also when the Lennard-Jones interactions are modified, although this does increase the solubility. When modifying the Lennard-Jones interactions, the three-phase coexistence temperature is between experimental values and the values reported by Costandy et al. at low pressures, but lower than both direct coexistence simulations as well as experimental values when pressures is higher than 1000 bar. Qualitatively, the phase diagram behaves the same when the Lennard-Jones interactions are, or are not mixed. It is clear that both the solubility of carbon dioxide in water, and the stability of the $CO_2$ hydrate are increased when the $\chi$-parameter is increased. Thus, our findings indicate that the current modification to Lennard-Jones interactions cannot at the same time be used to fit the $co_2$ solubility, and the stability of the $CO_2$ hydrate. This is similar to what was observed for a procedure where both the C−O and O−O interaction were modified by the same factor by Miguez et al.[17]

It is not clear that a simple model of carbon dioxide can be used to accurately model hydrate behavior, even with the inclusion of a mixing factor for water-$CO_2$ interactions. Working from ab-initio simulations, Klauda and Sandler[76] had found it necessary to use different Lennard-Jones parameters to describe the water-$CO_2$ interactions in small and large cages. This reflected the importance of many-body interactions, which depend on the different structures of the large and small cages. If it is necessary to modify the water-carbon dioxide interaction in a different manner when carbon dioxide is in a small or a large cage, it might also be necessary to adopt a third modification for when carbon dioxide is dissolved in liquid water. In contrast to Klauda and Sandler, Velega and Anderson[77] used ab-initio simulations to make a single set of fitted parameters for a carbon dioxide molecule based on the EPM2[78] model. In this case, the fitted param-

eters led to a degradation of the description of carbon dioxide in it's vapor phase. It is possible that this could have been avoided by making a fit of the mixing rules for water and carbon dioxide, rather than using Lorentz-Berthelot rules and only fitting the Lennard Jones parameters of the carbon dioxide molecule. Neither Klauda and Sandler nor Velega and Anderson reported solubility values for their models of carbon dioxide, so we can not make a direct evaluation on whether their modifications improved this.

Aimoli et al.[79] have made a comparative study of force fields for methane and carbon dioxide. Below 1000 bar, the density of TrAPPE $CO_2$ deviates from experimental carbon dioxide by $\sim 2-3\%$[79]. This deviation is higher near the critical point of $CO_2$. It is possible that a $CO_2$-model with a better description of the gas phase would improve the qualitative behavior of the phase diagram.

Since the modification of mixing rules is largely inspired by the need to account for the polarizability of molecules, better results might be obtained from explicitly polarizable models. Jiang et al.[80] recently developed a polarizable model of $CO_2$, and it would be interesting to see whether this can provide an improved description of the hydrate phase diagram.

The simulated carbon dioxide hydrate reaches a maximum temperature at a lower pressure than experimental values. It is possible that this premature retrograde behavior is similar in nature to the deviation from experimental results observed for methane hydrate at high pressures. This suggests that the premature retrograde behavior of the carbon dioxide hydrate is not only caused by the treatment of the water-$CO_2$ interactions, but also by the properties of the water model alone. We note that Miguez et al.[17] found a similar pressure shift for the retrograde behavior of TraPPE $CO_2$ mixed with TIP4P/Ice, using a mixing parameter $\chi = 1.13$ for all $CO_2$-$H_2O$ Lennard-Jones interactions, but not when the mixing parameter was unity.

There are two primary causes of the retrograde behavior. First, the volume difference between liquid water and the hydrate structure, which contributes to the Gibbs energy difference the quantity $P(V^{\mathrm{h}} - V^{\mathrm{l}}) + RT \ln(\frac{V^{\mathrm{h}}}{V^{\mathrm{l}}})$, which is approximately linear in pressure. Second, the compression of the cage structure starts to affect the adsorption isotherms, reducing the guests' contribution to the hydrate stability. The volume difference between hydrate and liquid phase, which is related to the enthalpy of dissociation, seems like the most likely reason for the premature retrograde behavior. Both the water models we have studied underpredict the density-difference between ice and liquid water[39], which in turn reduces the melting enthalpy. It seems reasonable that the misprediction of density also here is the cause of a distorted phase-diagram.

Even as the retrograde behavior starts to occur, the filling fraction of the metastable hydrate structure increases. This is evident from figures 6 and 7, where we have computed the fractional occupancy at the dissociation temperature for each pressure considered. Brumby et al.[81] computed methane occupancy in TIP4P/Ice hydrate for a wide range of pressures and temperatures, and found a deviation from the results of Jensen et al.[22] Our current results fit well with those of Brumby, implying that Jensen et al. overpredicted the amount of methane adsorbed in the hydrate. It seems likely that a systematic error occured when Jensen et al. computed the fugacity of methane, and that this is the cause of systematic errors.

# Conclusions

The phase diagram of OPLS-UA methane and TraPPE carbon dioxide hydrates has been computed for two water models, TIP4P/Ice and TIP4P/2005, purely by molecular Monte Carlo simulations. To determine the three-phase coexistence points, residual chemical potentials were calculated for all phases at several temperatures, using sev-

eral techniques, and a linear interpolation was used to find the temperature where the chemical potentials in all phases were equal. The obtained phase diagram for methane hydrates corresponds closely to direct coexistence simulations, as well as experimental values. For carbon dioxide, there is a systematic deviation from direct coexistence simulations. We propose that this deviation may be caused by the lack of tail corrections for Lennard-Jones interactions in direct coexistence simulations. The phase diagram of carbon dioxide hydrate exhibits a retrograde behavior at pressures that are somewhat lower than experimentally observed, while methane hydrates start deviating from experimental results at high pressures, in what could be indicative of a premature retrograde behavior. For carbon dioxide hydrates, this contradicts previous direct coexistence simulations. For methane hydrates, this pressure region is to our knowledge previously unstudied by reliable simulations. The dissociation entropies and enthalpies for OPLS-UA methane and TraPPE carbon dioxide hydrate for the TIP4P/Ice and TIP4P/2005 water models were provided. The computed coexistence points are found to be highly sensitive to systematic errors in the computed chemical potentials. With this work, we demonstrate a correct implementation of the technique. This sets up a framework for calculating driving forces of hydrate nucleation.

## Acknowledgements

This work has been funded by Statoil through grant 4502484658. Computational resources have been supplied by NOTUR, under project 4504k. TJHV acknowledges NWO-CW for a VICI grant. SK is grateful to the Research Council of Norway through its Centres of Excellence funding scheme, project number 262644.

## References

(1) Sloan Jr, E. D.; Koh, C. Clathrate Hydrates of Natural Gases; CRC press, 2007.

(2) Marshall, D. R.; Saito, S.; Kobayashi, R. Hydrates at High Pressures: Part I. Methane-Water, Argon-Water, and Nitrogen-Water Systems. AIChE J. 1964, 10, 202–205.

(3) Ohgaki, K.; Hamanaka, T. Phase-Behavior of $CO_2$ Hydrate-Liquid $CO_2$-$H_2O$ System at High Pressure. Kagaku Kogaku Ronbun. 1995, 21, 800–803.

(4) Nakano, S.; Moritoki, M.; Ohgaki, K. High-Pressure Phase Equilibrium and Raman Microprobe Spectroscopic Studies on the $CO_2$ Hydrate System. J. Chem. Eng. Data 1998, 43, 807–810.

(5) Kvenvolden, K. A. Gas Hydrates—Geological Perspective and Global Change. Rev. Geophys. 1993, 31, 173–187.

(6) Ohgaki, K.; Takano, K.; Sangawa, H.; Matsubara, T.; Nakano, S. Methane Exploitation by Carbon Dioxide from Gas Hydrates - Phase Equilibria for $CO_2$-$CH_4$ Mixed Hydrate System. J. Chem. Eng. Jpn. 1996, 29, 478–483.

(7) Kvamme, B.; Graue, A.; Buanes, T.; Kuznetsova, T.; Ersland, G. Storage of $CO_2$ in Natural Gas Hydrate Reservoirs and the Effect of Hydrate as an Extra Sealing in Cold Aquifers. Int. J. Greenh. Gas Control 2007, 1, 236 – 246, 8th International Conference on Greenhouse Gas Control Technologies GHGT-8.

(8) Chong, Z. R.; Yang, S. H. B.; Babu, P.; Linga, P.; Li, X.-S. Review of Natural Gas Hydrates as an Energy Resource: Prospects and Challenges. Appl. Energy 2016, 162, 1633 – 1652.

(9) Peng, D.-Y.; Robinson, D. B. A New Two-Constant Equation of State. Ind. Eng. Chem. Fundam. 1976, 15, 59–64.

(10) van der Waals, J. H.; Platteeuw, J. C. Clathrate Solutions. Advances in Chemical Physics 1959, 2, 1–57.

(11) Tanaka, H.; Kiyohara, K. On the Thermodynamic Stability of Clathrate Hydrate. I. J. Chem. Phys 1993, 98, 4098–4109.

(12) Jäger, A.; Vinš, V.; Gernert, J.; Span, R.; Hrubý, J. Phase Equilibria with Hydrate Formation in $H_2O$ + $CO_2$ Mixtures Modeled with Reference Equations of State. Fluid Phase Equilib. 2013, 338, 100 – 113.

(13) Vinš, V.; Jäger, A.; Span, R.; Hrubý, J. Model for Gas Hydrates Applied to CCS Systems Part I. Parameter Study of the van der Waals and Platteeuw model. Fluid Phase Equilib. 2016, 427, 268 – 281.

(14) Warrier, P.; Khan, M. N.; Srivastava, V.; Maupin, C. M.; Koh, C. A. Overview: Nucleation of Clathrate Hydrates. J. Chem. Phys 2016, 145, 211705.

(15) Conde, M. M.; Vega, C. Determining the Three-Phase Coexistence Line in Methane Hydrates using Computer Simulations. J. Chem. Phys 2010, 133, 064507.

(16) Michalis, V. K.; Costandy, J.; Tsimpanogiannis, I. N.; Stubos, A. K.; Economou, I. G. Prediction of the Phase Equilibria of Methane Hydrates using the Direct Phase Coexistence Methodology. J. Chem. Phys 2015, 142, 044501.

(17) Míguez, J. M.; Conde, M. M.; Torré, J.-P.; Blas, F. J.; Piñeiro, M. M.; Vega, C. Molecular Dynamics Simulation of $CO_2$ hydrates: Prediction of Three Phase Coexistence Line. J. Chem. Phys 2015, 142, 124505.

(18) Costandy, J.; Michalis, V. K.; Tsimpanogiannis, I. N.; Stubos, A. K.; Economou, I. G. The Role of Intermolecular Interactions in the Prediction of the Phase Equilibria of Carbon Dioxide Hydrates. J. Chem. Phys 2015, 143, 094506.

(19) Wierzchowski, S. J.; Monson, P. A. Calculating the Phase Behavior of Gas-Hydrate-Forming Systems from Molecular Models. Ind. Eng. Chem. Res. 2006, 45, 424–431.

(20) Nezbeda, I.; Smith, W. R.; Kolafa, J. Molecular Theory of Phase Equilibria in Model Associated Mixtures. I. Binary Mixtures of Water and a Simple Fluid. J. Chem. Phys 1994, 100, 2191–2201.

(21) Nezbeda, I.; Kolafa, J.; Pavlíček, J.; Smith, W. R. Molecular Theory of Phase Equilibria in Model and Real Associated Mixtures. II. Binary Aqueous Mixtures of Inert Gases and n-Alkanes. J. Chem. Phys 1995, 102, 9638–9646.

(22) Jensen, L.; Thomsen, K.; von Solms, N.; Wierzchowski, S.; Walsh, M. R.; Koh, C. A.; Sloan, E. D.; Wu, D. T.; Sum, A. K. Calculation of Liquid Water-Hydrate-Methane Vapor Phase Equilibria from Molecular Simulations. J. Phys. Chem. B 2010, 114, 5775–5782.

(23) Abascal, J. L. F.; Sanz, E.; García Fernández, R.; Vega, C. A Potential Model for the Study of Ices and Amorphous Water: TIP4P/Ice. J. Chem. Phys 2005, 122, 234511.

(24) Jorgensen, W. L.; Maxwell, D. S.; Tirado-Rives, J. Development and Testing of the OPLS All-Atom Force Field on Conformational Energetics and Properties of Organic Liquids. J. Am. Chem. Soc. 1996, 118, 11225–11236.

(25) Pimpalgaonkar, H.; Veesam, S. K.; Punnathanam, S. N. Theory of Gas Hydrates: Effect of the Approximation of Rigid Water Lattice. J. Phys. Chem. B 2011, 115, 10018–10026.

(26) Ravipati, S.; Punnathanam, S. N. Calculation of Three-Phase Methane–Ethane Binary Clathrate Hydrate Phase Equilibrium from Monte Carlo Molecular Simulations. Fluid Phase Equilib. 2014, 376, 193 – 201.

(27) Ravipati, S.; Punnathanam, S. N. Improving the Rigor and Consistency of the Thermodynamic Theory for Clathrate Hydrates through Incorporation of Move-

ment of Water Molecules of Hydrate Lattice. J. Phys. Chem. C 2015, 119, 12365–12377.

(28) Ladd, A.; Woodcock, L. Triple-Point Coexistence Properties of the Lennard-Jones System. Chem. Phys. Lett. 1977, 51, 155 – 159.

(29) Noya, E. G.; Vega, C.; de Miguel, E. Determination of the Melting Point of Hard Spheres from Direct Coexistence Simulation Methods. J. Chem. Phys 2008, 128, 154507.

(30) Fernández, R. G.; Abascal, J. L. F.; Vega, C. The Melting Point of Ice Ih for Common Water Models Calculated from Direct Coexistence of the Solid-Liquid Interface. J. Chem. Phys 2006, 124, 144506.

(31) Espinosa, J. R.; Sanz, E.; Valeriani, C.; Vega, C. On Fluid-Solid Direct Coexistence Simulations: The Pseudo-Hard Sphere Model. J. Chem. Phys 2013, 139, 144502.

(32) Noya, E. G.; Kolovos, I.; Doppelbauer, G.; Kahl, G.; Bianchi, E. Phase Diagram of Inverse Patchy Colloids Assembling into an Equilibrium Laminar Phase. Soft Matter 2014, 10, 8464–8474.

(33) Luis, D.; López-Lemus, J.; Maspoch, M. L.; Franco-Urquiza, E.; Saint-Martin, H. Methane Hydrate: Shifting the Coexistence Temperature to Higher Temperatures with an External Electric Field. Mol. Simul. 2016, 42, 1014–1023.

(34) Smirnov, G. S.; Stegailov, V. V. Melting and Superheating of sI Methane Hydrate: Molecular Dynamics Study. J. Chem. Phys 2012, 136, 044523.

(35) Michalis, V. K.; Tsimpanogiannis, I. N.; Stubos, A. K.; Economou, I. G. Direct Phase Coexistence Molecular Dynamics Study of the Phase Equilibria of the Ternary Methane-Carbon Dioxide-Water Hydrate System. Phys. Chem. Chem. Phys. 2016, 18, 23538–23548.

(36) Wierzchowski, S. J.; Monson, P. A. Calculation of Free Energies and Chemical Potentials for Gas Hydrates Using Monte Carlo Simulations. J. Phys. Chem. B 2007, 111, 7274–7282.

(37) Sanz, E.; Vega, C.; Abascal, J. L. F.; MacDowell, L. G. Phase Diagram of Water from Computer Simulation. Phys. Rev. Lett. 2004, 92, 255701.

(38) Allen, M.; Tildesley, D. Computer Simulation of Liquids. 1987,

(39) Abascal, J. L. F.; Vega, C. A General Purpose Model for the Condensed Phases of Water: TIP4P/2005. J. Chem. Phys 2005, 123, 234505.

(40) Potoff, J. J.; Siepmann, J. I. Vapor–Liquid Equilibria of Mixtures Containing Alkanes, Carbon Dioxide, and Nitrogen. AIChE Journal 2001, 47, 1676–1682.

(41) Docherty, H.; Galindo, A.; Vega, C.; Sanz, E. A Potential Model for Methane in Water Describing Correctly the Solubility of the Gas and the Properties of the Methane Hydrate. J. Chem. Phys 2006, 125, 074510.

(42) Orozco, G. A.; Economou, I. G.; Panagiotopoulos, A. Z. Optimization of Intermolecular Potential Parameters for the $CO_2/H_2O$ Mixture. J. Phys. Chem. B 2014, 118, 11504–11511.

(43) Frenkel, D.; Smit, B. Understanding Molecular Simulation: From Algorithms to Applications; Academic press, 2001.

(44) Johnson, J. K.; Zollweg, J. A.; Gubbins, K. E. The Lennard-Jones Equation of State Revisited. Mol. Phys. 1993, 78, 591–618.

(45) McMullan, R. K.; Jeffrey, G. A. Polyhedral Clathrate Hydrates. IX. Structure of Ethylene Oxide Hydrate. J. Chem. Phys 1965, 42, 2725–2732.

(46) Takeuchi, F.; Hiratsuka, M.; Ohmura, R.; Alavi, S.; Sum, A. K.; Yasuoka, K. Water Proton Configurations in Structures I, II, and H Clathrate Hydrate Unit Cells. J. Chem. Phys 2013, 138, 124504.

(47) Vega, C.; Monson, P. A. Solid–Fluid Equilibrium for a Molecular Model with Short Ranged Directional Forces. J. Chem. Phys 1998, 109, 9938–9949.

(48) Frenkel, D.; Ladd, A. J. C. New Monte Carlo Method to Compute the Free Energy of Arbitrary Solids. Application to the fcc and hcp Phases of Hard Spheres. J. Chem. Phys 1984, 81, 3188–3193.

(49) Polson, J. M.; Trizac, E.; Pronk, S.; Frenkel, D. Finite-Size Corrections to the Free Energies of Crystalline Solids. J. Chem. Phys 2000, 112, 5339–5342.

(50) Vega, C.; Monson, P. A. Erratum: Solid-Fluid Equilibrium for a Molecular Model with Short Ranged Directional Forces [J. Chem. Phys.109, 9938 (1998)]. J. Chem. Phys 2006, 125, 109901.

(51) Nagle, J. F. Lattice Statistics of Hydrogen Bonded Crystals. I. The Residual Entropy of Ice. J.Math.Phys. 1966, 7, 1484–1491.

(52) Shi, W.; Maginn, E. J. Continuous Fractional Component Monte Carlo: An Adaptive Biasing Method for Open System Atomistic Simulations. J. Chem. Theory Comput. 2007, 3, 1451–1463.

(53) Wang, F.; Landau, D. P. Efficient, Multiple-Range Random Walk Algorithm to Calculate the Density of States. Phys. Rev. Lett. 2001, 86, 2050–2053.

(54) Torres-Knoop, A.; Balaji, S. P.; Vlugt, T. J. H.; Dubbeldam, D. A Comparison of Advanced Monte Carlo Methods for Open Systems: CFCMC vs CBMC. J. Chem. Theory Comput. 2014, 10, 942–952.

(55) Poursaeidesfahani, A.; Rahbari, A.; Torres-Knoop, A.; Dubbeldam, D.; Vlugt, T. J. H. Computation of Thermodynamic Properties in the Continuous Fractional Component Monte Carlo Gibbs Ensemble. Mol Simul 2017, 43, 189–195.

(56) Torres-Knoop, A.; Poursaeidesfahani, A.; Vlugt, T. J. H.; Dubbeldam, D. Behavior of the Enthalpy of Adsorption in Nanoporous Materials Close to Saturation Conditions. J. Chem. Theory Comput. 0, 0, null.

(57) Carroll, J. J.; Mather, A. E. The System Carbon Dioxide-Water and the Krichevsky-Kasarnovsky Equation. J. Solution Chem. 1992, 21, 607–621.

(58) Zhang, Y. I.; Jain, P.; Chen, R.; Elliot, D.; Song, K.; Chapman, W.; Kobayashi, R.; Ng, H.-J. In Advances in the Study of Gas Hydrates; Taylor, C. E., Kwan, J. T., Eds.; Springer US: Boston, MA, 2004; pp 157–171.

(59) Prini, R. F.; Crovetto, R. Evaluation of Data on Solubility of Simple Apolar Gases in Light and Heavy Water at High Temperature. J. Phys. Chem. Ref. Data 1989, 18, 1231–1243.

(60) Fernández-Prini, R.; Alvarez, J. L.; Harvey, A. H. Henry's Constants and Vapor–Liquid Distribution Constants for Gaseous Solutes in $H_2O$ and $D_2O$ at High Temperatures. J. Phys. Chem. Ref. Data 2003, 32, 903–916.

(61) Moore, J. C.; Battino, R.; Rettich, T. R.; Handa, Y. P.; Wilhelm, E. Partial Molar Volumes of Gases at Infinite Dilution in Water at 298.15 K. J. Chem. Eng. Data 1982, 27, 22–24.

(62) Rettich, T. R.; Handa, Y. P.; Battino, R.; Wilhelm, E. Solubility of Gases in Liquids. 13. High-Precision Determination of Henry's Constants for Methane and Ethane in Liquid Water at 275 to 328 K. J. Phys. Chem. 1981, 85, 3230–3237.

(63) Vilseck, J. Z.; Tirado-Rives, J.; Jorgensen, W. L. Determination of Partial Molar Volumes from Free Energy Perturbation Theory. Phys. Chem. Chem. Phys. 2015, 17, 8407–8415.

(64) Moghaddam, M. S.; Chan, H. S. Pressure and Temperature Dependence of Hydrophobic Hydration: Volumetric, Compressibility, and Thermodynamic Signatures. J. Chem. Phys 2007, 126, 114507.

(65) Martin, M. G.; Siepmann, J. I. Transferable Potentials for Phase Equilibria. 1. United-Atom Description of n-Alkanes. J. Phys. Chem. B 1998, 102, 2569–2577.

(66) McBride-Wright, M.; Maitland, G. C.; Trusler, J. P. M. Viscosity and Density of Aqueous Solutions of Carbon Dioxide at Temperatures from (274 to 449) K and at Pressures up to 100 MPa. J. Chem. Eng. Data 2015, 60, 171–180.

(67) Duan, Z.; Sun, R.; Zhu, C.; Chou, I.-M. An Improved Model for the Calculation of $CO_2$ Solubility in Aqueous Solutions Containing $Na^+$, $K^+$, $Ca^{2+}$, $Mg^{2+}$, $Cl^-$, and $SO_4^{2-}$. Mar. Chem. 2006, 98, 131 – 139.

(68) Moustafa, S. G.; Schultz, A. J.; Kofke, D. A. Effects of Finite Size and Proton Disorder on Lattice-Dynamics Estimates of the Free Energy of Clathrate Hydrates. Ind. Eng. Chem. Res. 2015, 54, 4487–4496.

(69) Gupta, A.; Lachance, J.; Jr., E. S.; Koh, C. A. Measurements of Methane Hydrate Heat of Dissociation using High Pressure Differential Scanning Calorimetry. Chem. Eng. Sci. 2008, 63, 5848 – 5853.

(70) Anderson, G. K. Enthalpy of Dissociation and Hydration Number of Carbon Dioxide Hydrate from the Clapeyron Equation. J. Chem. Thermodyn. 2003, 35, 1171 – 1183.

(71) Loveday, J. S.; Nelmes, R. J. High-pressure Gas Hydrates. Phys. Chem. Chem. Phys. 2008, 10, 937–950.

(72) Janeček, J. Long Range Corrections in Inhomogeneous Simulations. J. Chem. Phys. B 2006, 110, 6264–6269.

(73) Goujon, F.; Ghoufi, A.; Malfreyt, P.; Tildesley, D. J. Controlling the Long-Range Corrections in Atomistic Monte Carlo Simulations of Two-Phase Systems. J. Chem. Theory Comput. 2015, 11, 4573–4585.

(74) Manzanilla-Granados, H. M.; Saint-Martín, H.; Fuentes-Azcatl, R.; Alejandre, J. Direct Coexistence Methods to Determine the Solubility of Salts in Water from Numerical Simulations. Test Case NaCl. J. Chem. Phys. B 2015, 119, 8389–8396.

(75) Nezbeda, I.; Moučka, F.; Smith, W. R. Recent Progress in Molecular Simulation of Aqueous Electrolytes: Force Fields, Chemical Potentials and Solubility. Mol. Phys. 2016, 114, 1665–1690.

(76) Klauda, J. B.; Sandler, S. I. Ab Initio Intermolecular Potentials for Gas Hydrates and Their Predictions. J. Phys. Chem. B 2002, 106, 5722–5732.

(77) Velaga, S. C.; Anderson, B. J. Carbon Dioxide Hydrate Phase Equilibrium and Cage Occupancy Calculations Using Ab Initio Intermolecular Potentials. J. Phys. Chem. B 2014, 118, 577–589.

(78) Harris, J. G.; Yung, K. H. Carbon Dioxide's Liquid-Vapor Coexistence Curve And Critical Properties as Predicted by a Simple Molecular Model. J. Phys. Chem. 1995, 99, 12021–12024.

(79) Aimoli, C. G.; Maginn, E. J.; Abreu, C. R. Force Field Comparison and Thermodynamic Property Calculation of Supercritical $CO_2$ and $CH_4$ using Molecular Dynamics Simulations. Fluid Phase Equilib. 2014, 368, 80 – 90.

(80) Jiang, H.; Moultos, O. A.; Economou, I. G.; Panagiotopoulos, A. Z. Gaussian-Charge Polarizable and Nonpolarizable Models for $CO_2$. J. Phys. Chem. B 2016, 120, 984–994.

(81) Brumby, P. E.; Yuhara, D.; Wu, D. T.; Sum, A. K.; Yasuoka, K. Cage Occupancy of Methane Hydrates from Gibbs Ensemble Monte Carlo Simulations. Fluid Phase Equilib. 2016, 413, 242 – 248, Special Issue: Gas Hydrates and Semiclathrate Hydrates.

(82) Perry, R. H.; Green, D. W. Perry's Chemical Engineers' Handbook; McGraw-Hill Professional, 1999.

# List of Tables

Table 1: Water models used in this work. TIP4P/Ice[23] and TIP4P/2005[39] are four-site models, for which the negative charge is placed on a virtual atom (M), located along the bisection of the HOH angle.

| Water Model | Atom | $\sigma$/Å | $\epsilon$/kJ $\cdot$ mol$^{-1}$ | $q$/e | $d_{OH}$/Å | $d_{OM}$/Å | $\phi_{HOH}$ |
|---|---|---|---|---|---|---|---|
| TIP4P/Ice | O | 3.1668 | 0.0.8822 | - | 0.9572 | 0.15 | 104.52 |
| | H | - | - | 0.5897 | | | |
| | M | - | - | -1.1794 | | | |
| TIP4P/2005 | O | 3.1589 | 0.7749 | - | 0.9572 | 0.1546 | 104.52 |
| | H | - | - | 0.5564 | | | |
| | M | - | - | -1.1128 | | | |

Table 2: Force fields of TraPPE[40] carbon dioxide and OPLS-UA methane[24] Methane is a single-site Lennard-Jones particle, while carbon dioxide is a linear 3-site molecule with charges and Lennard-Jones interaction sites on all atoms. Mixing parameters $\chi$ that are fitted so that the solubility of the models in liquid water corresponds to experimental values[18,41]

| Molecule | Atom | $\sigma$/Å | $\epsilon$/kJ $\cdot$ mol$^{-1}$ | $q$/e | $d_{CO}$/Å | $\chi_{2005}$ | $\chi_{Ice}$ |
|---|---|---|---|---|---|---|---|
| Methane | CH4 | 3.730 | 1.23053 | - | - | 1.07[41] | 1.00[15] |
| Carbon | C | 2.800 | 0.22449 | 0.7 | 1.16 | - | - |
| dioxide | O | 3.050 | 0.65684 | -0.35 | | 1.115[18] | 1.08[18] |

Table 3: Critical pressures $P_c$, temperatures $T_c$, and acentric factors $\omega$ used in evaluating the Peng-Robinson[9] equation of state for TraPPE[40] carbon dioxide and OPLS-UA[24] methane. Critical properties from Refs. [40,65]. Acentric factors from Ref. [82]

| Molecule | $P_c$/bar | $T_c$/K | $\omega$ |
|---|---|---|---|
| $CH_4$ | 45 | 191.4 | 0.011 |
| $CO_2$ | 77.7 | 306.2 | 0.224 |

Table 4: Three phase equilibrium temperature $T$, as a function of pressure, $P$ of methane hydrate, as simulated with the OPLS-UA model of methane, and the TIP4P/Ice and TIP4P/2005 water models. The mixing parameter $\chi$ modifies the Lennard Jones interaction between the water oxygen atom and $CH_4$. Numbers in parentheses indicate the error in the last (two) digits.

| Water model | TIP4P/2005 | | TIP4P/Ice |
|---|---|---|---|
| $\chi$ | 1.0 | 1.07 | 1.0 |
| $P$/bar | | $T$/K | |
| 50 | 261.27(0.16) | 268.01(0.13) | 278(2) |
| 100 | 267.6(0.3) | 274.5(0.5) | 286.5(1.4) |
| 200 | 273.03(0.07) | 280.4(0.2) | 293.4(1.1) |
| 500 | 278.2(0.6) | 286.1(0.9) | 300.0(1.2) |
| 1000 | 283.5(0.8) | 292.0(1.1) | 304.7(0.5) |
| 2000 | 289.1(0.5) | 297.6(0.8) | 310.0(0.6) |
| 4000 | - | - | 312.4(0.7) |

Table 5: Three phase equilibrium temperature $T$, as a function of pressure, $P$ of carbon dioxide hydrate, as simulated with the TraPPE model of carbon dioxide[40], and the TIP4P/Ice[23] and TIP4P/2005[39] water models. The mixing parameter $\chi$ modifies the Lennard Jones interaction between the water oxygen atom and $CO_2$ oxygen atoms. Numbers in parentheses indicate the error in the last (two) digits.

| Water model | TIP4P/2005 | | TIP4P/Ice | |
|---|---|---|---|---|
| $\chi$ | 1.0 | 1.115 | 1.0 | 1.08 |
| $P$/bar | $T$/K | | | |
| 50 | 252.6(0.4) | 262.5(0.2) | 276(4) | 283(2) |
| 100 | 253.2(0.9) | 262.8(0.5) | 275(4) | 283(2) |
| 200 | 253.3(0.3) | 263.29(0.10) | 276(3) | 283.9(1.7) |
| 500 | 254.6(0.6) | 264.8(0.3) | 277(2) | 284.8(0.9) |
| 1000 | 255.6(0.5) | 266.3(0.2) | 279.3(0.5) | 287.0(0.3) |
| 2000 | 257.2(0.4) | 268.0(0.3) | 281.2(0.8) | 288.9(0.4) |
| 4000 | - | - | 278.7(0.7) | 287.45(0.18) |

Table 6: Dissociation enthalpy, $\Delta_m H$, and entropy, $\Delta_d S$, per mol water of methane hydrate at pressure $P$ and corresponding three phase equilibrium temperature $T$ for OPLS-UA methane[24] and TIP4P/2005 water[39].

| $P$ | $T$ | $\Delta_d S/\mathrm{J \cdot K^{-1} mol^{-1}}$ | $\Delta_d H/\mathrm{kJ \cdot mol^{-1}}$ |
|---|---|---|---|
| 50 | 261.2 | 29.4(0.6) | 7.70(0.07) |
| 100 | 267.6 | 29.5(1.3) | 7.91(0.17) |
| 200 | 273.0 | 27.3(0.1) | 7.48(0.02) |
| 500 | 278.1 | 26.6(1.0) | 7.42(0.13) |
| 1000 | 283.4 | 25.6(1.0) | 7.27(0.13) |
| 2000 | 289.0 | 25.2(0.5) | 7.28(0.06) |

Table 7: Dissociation enthalpy, $\Delta_m H$, and entropy, $\Delta_d S$, per mol water of methane hydrate at pressure $P$ and corresponding three phase equilibrium temperature $T$ for OPLS-UA methane[24] and TIP4P/2005[39] water with a mixing parameter $\chi = 1.07$ modifying the methane-water oxygen Lennard-Jones interaction.

| $P$ | $T$ | $\Delta_d S/\mathrm{J \cdot K^{-1} mol^{-1}}$ | $\Delta_d H/\mathrm{kJ \cdot mol^{-1}}$ |
|---|---|---|---|
| 50 | 268.0 | 30.3(0.5) | 8.14(0.07) |
| 100 | 274.4 | 30.1(1.1) | 8.26(0.15) |
| 200 | 280.4 | 27.9(0.2) | 7.84(0.03) |
| 500 | 286.1 | 26.8(1.1) | 7.69(0.14) |
| 1000 | 291.9 | 25.6(1.0) | 7.49(0.13) |
| 2000 | 297.6 | 25.3(0.6) | 7.54(0.08) |

Table 8: Dissociation enthalpy, $\Delta_m H$, and entropy, $\Delta_d S$, per mol water of carbon dioxide hydrate at pressure $P$ and corresponding three phase equilibrium temperature $T$ for TraPPE carbon dioxide[40] and TIP4P/2005[39] water.

| $P$ | $T$ | $\Delta_d S/\mathrm{J \cdot K^{-1} mol^{-1}}$ | $\Delta_d H/\mathrm{kJ \cdot mol^{-1}}$ |
|---|---|---|---|
| 50 | 252.6 | 22.3(0.5) | 5.63(0.07) |
| 100 | 253.2 | 23.0(1.4) | 5.84(0.17) |
| 200 | 253.3 | 22.3(0.4) | 5.65(0.05) |
| 500 | 254.5 | 22.7(1.0) | 5.78(0.12) |
| 1000 | 255.6 | 22.5(0.9) | 5.76(0.11) |
| 2000 | 257.1 | 22.6(0.8) | 5.81(0.10) |

Table 9: Dissociation enthalpy, $\Delta_m H$, and entropy, $\Delta_d S$, per mol water of carbon dioxide hydrate at pressure $P$ and corresponding three phase equilibrium temperature $T$ for TraPPE carbon dioxide[40] and TIP4P/2005[39] water. A mixing parameter $\chi = 1.115$ modified the Lennard-Jones interaction between the oxygen atoms of carbon dioxide and the oxygen atom of water.

| $P$ | $T$ | $\Delta_d S/\mathrm{J \cdot K^{-1} mol^{-1}}$ | $\Delta_d H/\mathrm{kJ \cdot mol^{-1}}$ |
|---|---|---|---|
| 50 | 262.4 | 23.0(0.6) | 6.05(0.08) |
| 100 | 262.7 | 23.3(1.4) | 6.12(0.19) |
| 200 | 263.2 | 22.6(0.3) | 5.97(0.04) |
| 500 | 264.7 | 23.2(0.9) | 6.16(0.12) |
| 1000 | 266.2 | 22.8(0.7) | 6.07(0.09) |
| 2000 | 268.0 | 22.4(0.7) | 6.02(0.10) |

Table 10: Dissociation enthalpy, $\Delta_m H$, and entropy, $\Delta_d S$, per mol water of carbon dioxide hydrate at pressure $P$ and corresponding three phase equilibrium temperature $T$ for TraPPE carbon dioxide[40] and TIP4P/Ice[23] water.

| $P$ | $T$ | $\Delta_d S/\mathrm{J \cdot K^{-1} mol^{-1}}$ | $\Delta_d H/\mathrm{kJ \cdot mol^{-1}}$ |
|---|---|---|---|
| 50 | 275.5 | 22(4) | 6.2(0.50) |
| 100 | 274.7 | 19(5) | 5.3(0.6) |
| 200 | 275.7 | 20(4) | 5.6(0.5) |
| 500 | 276.7 | 21(2) | 5.8(0.3) |
| 1000 | 279.2 | 22.6(0.9) | 6.33(0.12) |
| 2000 | 281.1 | 23.2(1.5) | 6.5(0.2) |
| 4000 | 278.6 | 22.4(1.1) | 6.25(0.14) |

Table 11: Dissociation enthalpy, $\Delta_m H$, and entropy, $\Delta_d S$, per mol water of carbon dioxide hydrate at pressure $P$ and corresponding three phase equilibrium temperature $T$ for TraPPE carbon dioxide[40] and TIP4P/Ice[23] water. A mixing parameter $\chi = 1.08$ modified the Lennard-Jones interaction between the oxygen atoms of carbon dioxide and the oxygen atom of water.

| $P$ | $T$ | $\Delta_d S/\mathrm{J \cdot K^{-1} mol^{-1}}$ | $\Delta_d H/\mathrm{kJ \cdot mol^{-1}}$ |
|---|---|---|---|
| 50 | 282.8 | 23(4) | 6.4(0.6) |
| 100 | 282.9 | 19(5) | 5.5(0.6) |
| 200 | 283.8 | 20(4) | 5.8(0.5) |
| 500 | 284.8 | 21(2) | 6.0(0.3) |
| 1000 | 286.9 | 22.7(0.8) | 6.54(0.11) |
| 2000 | 288.8 | 22.6(1.3) | 6.54(0.19) |
| 4000 | 287.4 | 22.8(0.5) | 6.55(0.07) |

Table 12: Solubility of TraPPE carbon dioxide[40] in TIP4P/2005[39] water as measured from CFCMC simulations. Uncertainties are less than 0.002.

| $P$/bar | $T$/K | | | | |
|---|---|---|---|---|---|
| | 255 | 260 | 265 | 270 | 275 |
| 50 | 0.018 | 0.016 | 0.014 | 0.014 | 0.014 |
| 100 | 0.018 | 0.015 | 0.015 | 0.015 | 0.014 |
| 200 | 0.020 | 0.018 | 0.017 | 0.016 | 0.014 |
| 500 | 0.022 | 0.019 | 0.019 | 0.017 | 0.016 |
| 1000 | 0.023 | 0.022 | 0.021 | 0.019 | 0.018 |
| 2000 | 0.025 | 0.020 | 0.019 | 0.020 | 0.018 |

Table 13: Solubility of TraPPE carbon dioxide[40] in TIP4P/2005[39] water as measured from CFCMC simulations. Lennard-Jones interactions between $CO_2$ oxygen and water oxygen atoms have been modified by a factor $\chi = 1.115$. Uncertainties are less than 0.002.

| $P$/bar | $T$/K | | | | |
|---|---|---|---|---|---|
| | 255 | 260 | 265 | 270 | 275 |
| 50 | 0.033 | 0.032 | 0.031 | 0.030 | 0.028 |
| 100 | 0.034 | 0.031 | 0.030 | 0.028 | 0.027 |
| 200 | 0.037 | 0.032 | 0.034 | 0.029 | 0.029 |
| 500 | 0.039 | 0.036 | 0.035 | 0.032 | 0.030 |
| 1000 | 0.041 | 0.042 | 0.038 | 0.037 | 0.034 |
| 2000 | 0.048 | 0.046 | 0.040 | 0.041 | 0.036 |

Table 14: Solubility of TraPPE carbon dioxide[40] in TIP4P/Ice[23] water as measured from CFCMC simulations. Uncertainties are less than 0.002.

| $P$/bar | $T$/K | | | | |
|---|---|---|---|---|---|
| | 280 | 285 | 290 | 295 | 300 |
| 50 | 0.016 | 0.015 | 0.013 | – | – |
| 100 | 0.015 | 0.015 | 0.014 | 0.014 | 0.012 |
| 200 | 0.018 | 0.016 | 0.014 | 0.014 | 0.014 |
| 500 | 0.020 | 0.019 | 0.017 | 0.016 | 0.015 |
| 1000 | 0.023 | 0.018 | 0.019 | 0.018 | 0.017 |
| 2000 | 0.024 | 0.019 | 0.022 | 0.020 | 0.017 |
| 4000 | 0.022 | 0.023 | 0.017 | 0.019 | 0.018 |

Table 15: Solubility of TraPPE carbon dioxide[40] in TIP4P/Ice[23] water as measured from CFCMC simulations. Lennard-Jones interactions between $CO_2$ oxygen and water oxygen atoms have been modified by a factor $\chi = 1.08$. Uncertainties are less than 0.002.

| $P$/bar | $T$/K | | | | |
|---|---|---|---|---|---|
| | 280 | 285 | 290 | 295 | 300 |
| 50 | 0.026 | 0.025 | 0.021 | – | – |
| 100 | 0.026 | 0.025 | 0.023 | 0.022 | 0.019 |
| 200 | 0.027 | 0.024 | 0.024 | 0.024 | 0.021 |
| 500 | 0.032 | 0.031 | 0.028 | 0.025 | 0.025 |
| 1000 | 0.036 | 0.033 | 0.033 | 0.030 | 0.026 |
| 2000 | 0.043 | 0.036 | 0.035 | 0.035 | 0.028 |
| 4000 | 0.031 | 0.031 | 0.032 | 0.029 | 0.030 |

# List of Figures

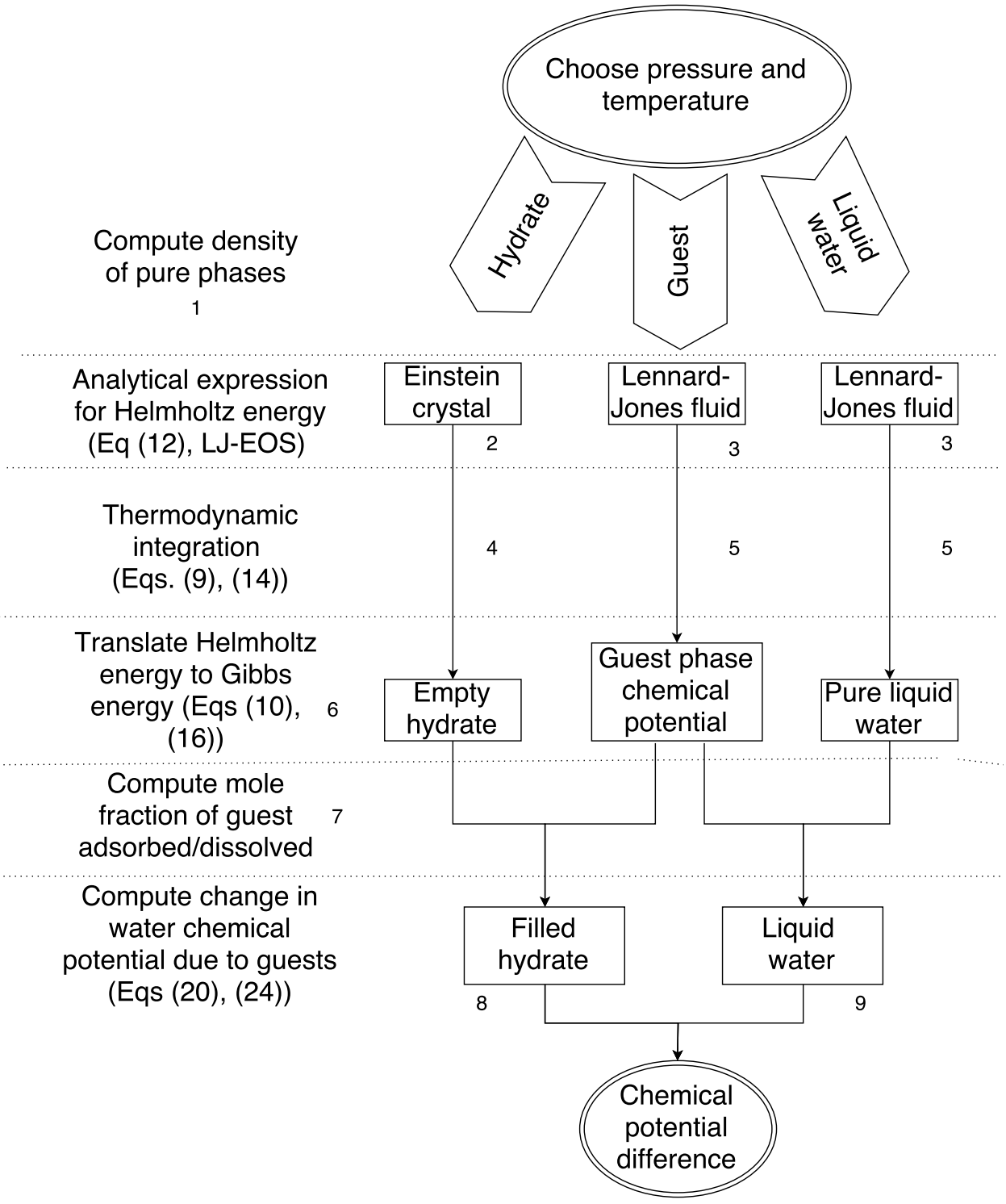


Figure 1: Flowchart describing how to compute the chemical potential difference betwen liquid water and hydrate, in contact with a third guest phase.

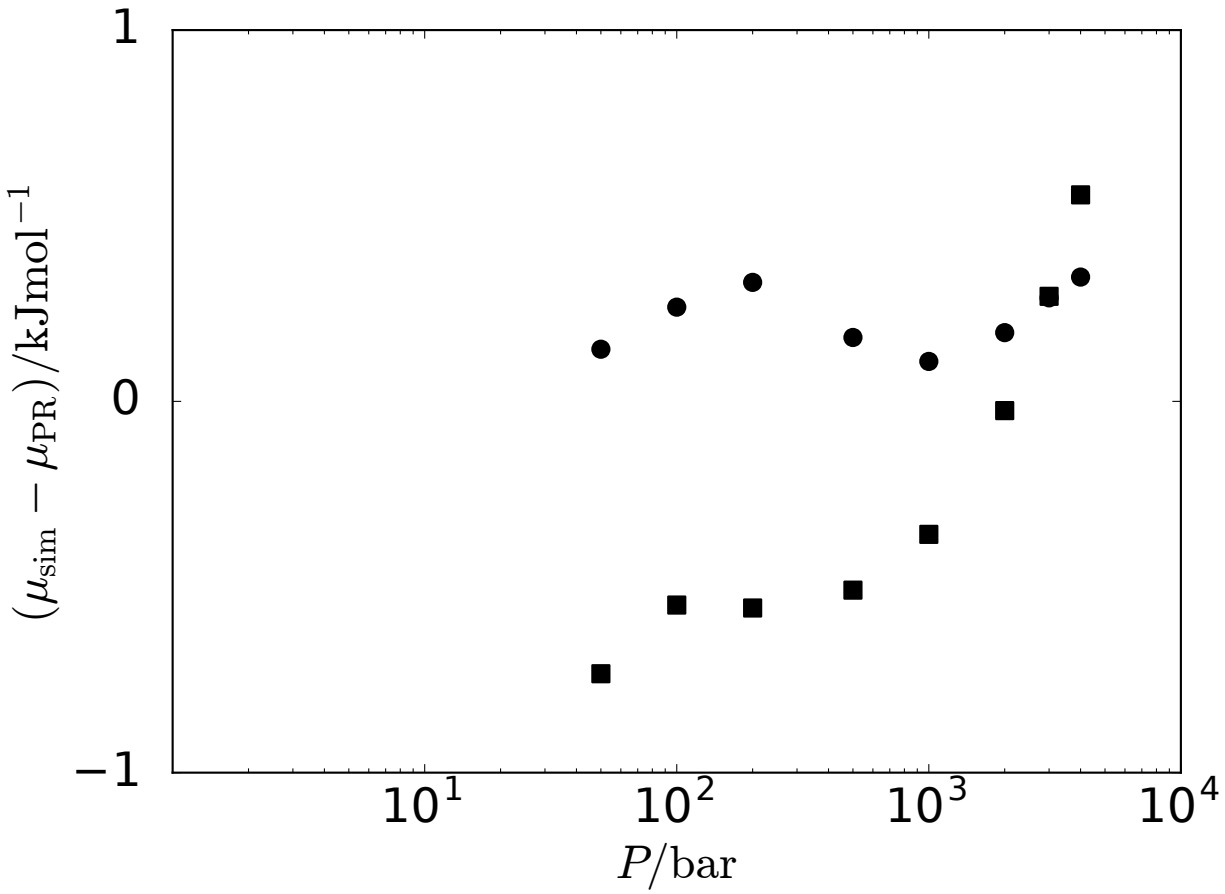


Figure 2: Difference in chemical potential as computed from simulation (sim) or the Peng-Robinson equation of state[9] (PR). Squares: Carbon dioxide. Circles: Methane.

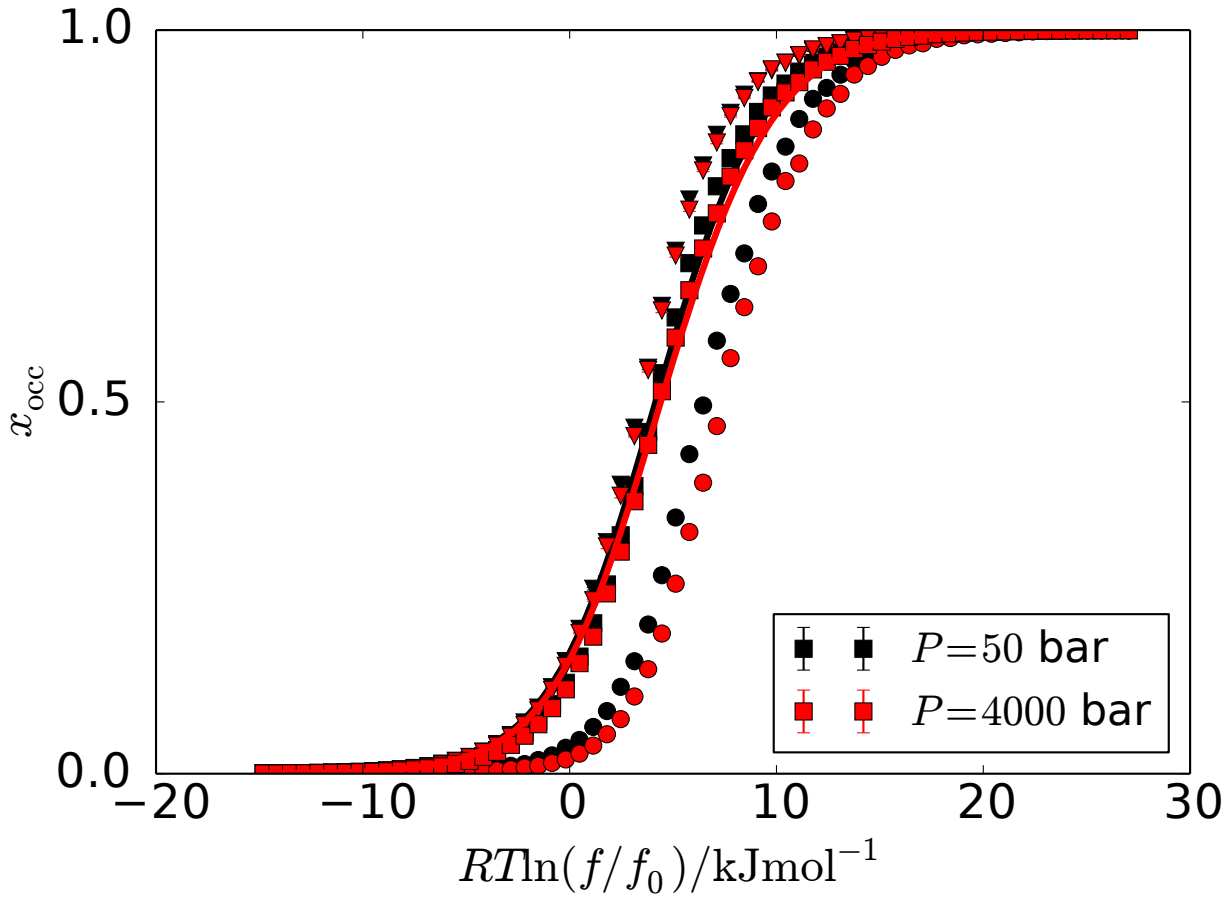


Figure 3: Fractional occupancy $x_{\mathrm{occ}}$ of sI hydrate (simulated using the TIP4P/Ice[23] water model), as a function of fugacity $f$, at 290 K and 50 and 4000 bar. Triangles represent the fractional occupancy of the large cages, circles the small cages, while squares represent the total fractional occupancy. The hydrate is filled by OPLS-UA methane[24]. The adsorption isotherms for the two different pressures are virtually indistinguishable.

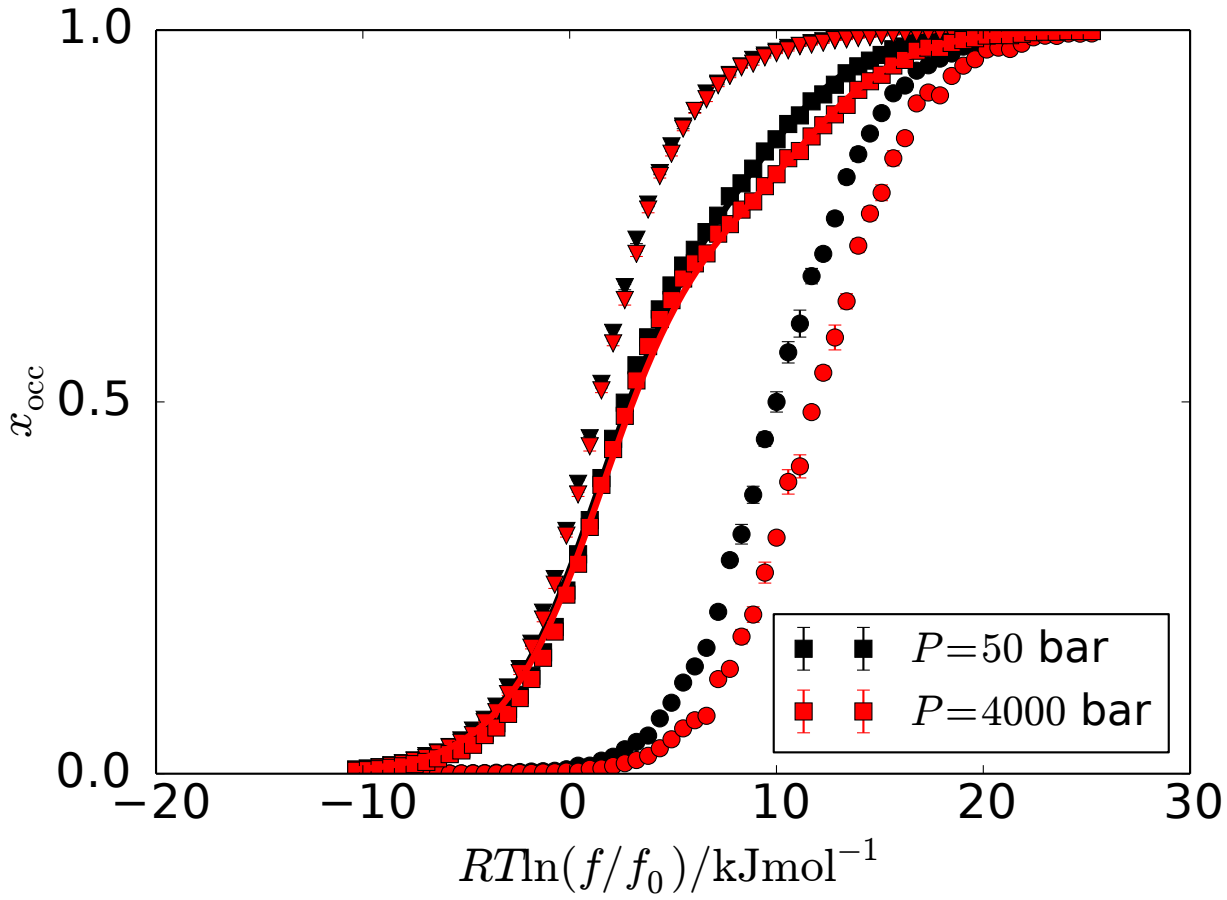


Figure 4: Fractional occupancy $x_{\mathrm{occ}}$ of sI hydrate (simulated using the TIP4P/Ice[23] water model), as a function of fugacity $f$, at 290 K and 50 and 4000 bar. Triangles represent the fractional occupancy of the large cages, circles the small cages, while squares represent the total fractional occupancy. The hydrate is filled by TraPPE carbon dioxide[40]. At 4000 bar, the adsorption isotherm corresponding to the small cage has shifted slightly to higher values, indicating that higher chemical potentials are required to fill the cages.

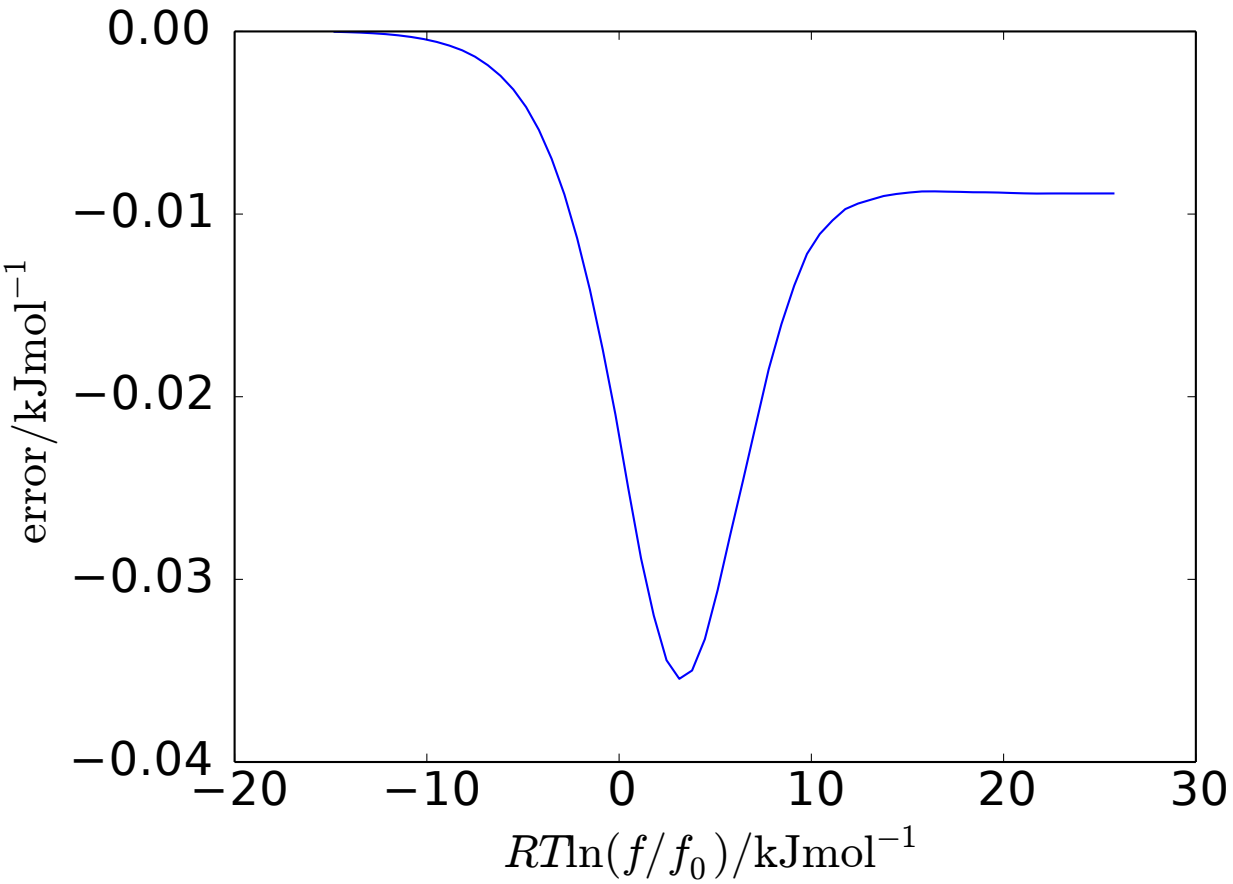


Figure 5: The error in water chemical potential due to integrating the adsorption curve analytically, via a fitted Langmuir-isotherm, equation (19), rather than numerically via measured occupancies. Evaluated for methane at 4000 bar and 290 K, different guests and conditions observe similar behavior.

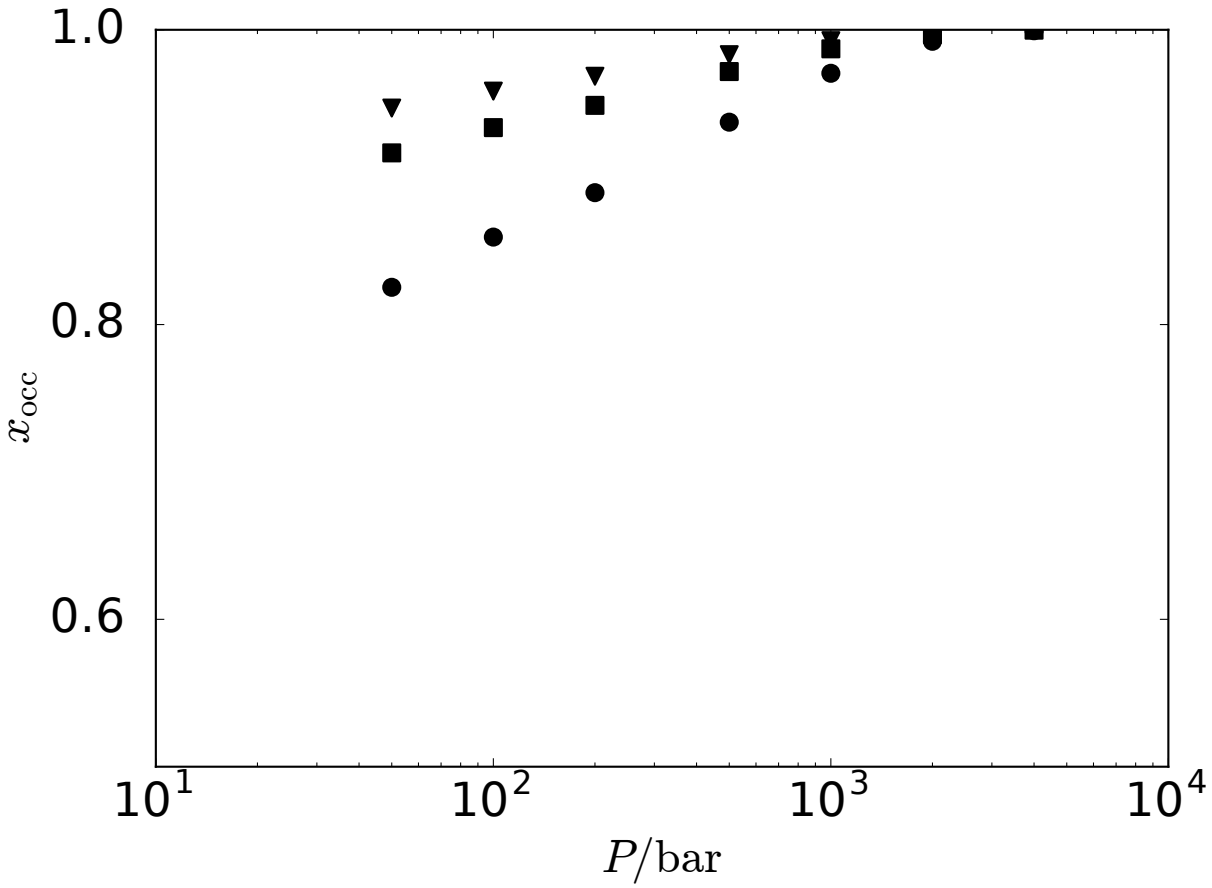


Figure 6: Fractional occupancy $x_{\mathrm{occ}}$ of OPLS-UA methane[24] in sI hydrate (simulated using the TIP4P/Ice[23]water model), as a function of pressure $f$, at the dissociation temperature. Triangles represent the fractional occupancy of the large cages, circles the small cages, while squares represent the total fractional occupancy.

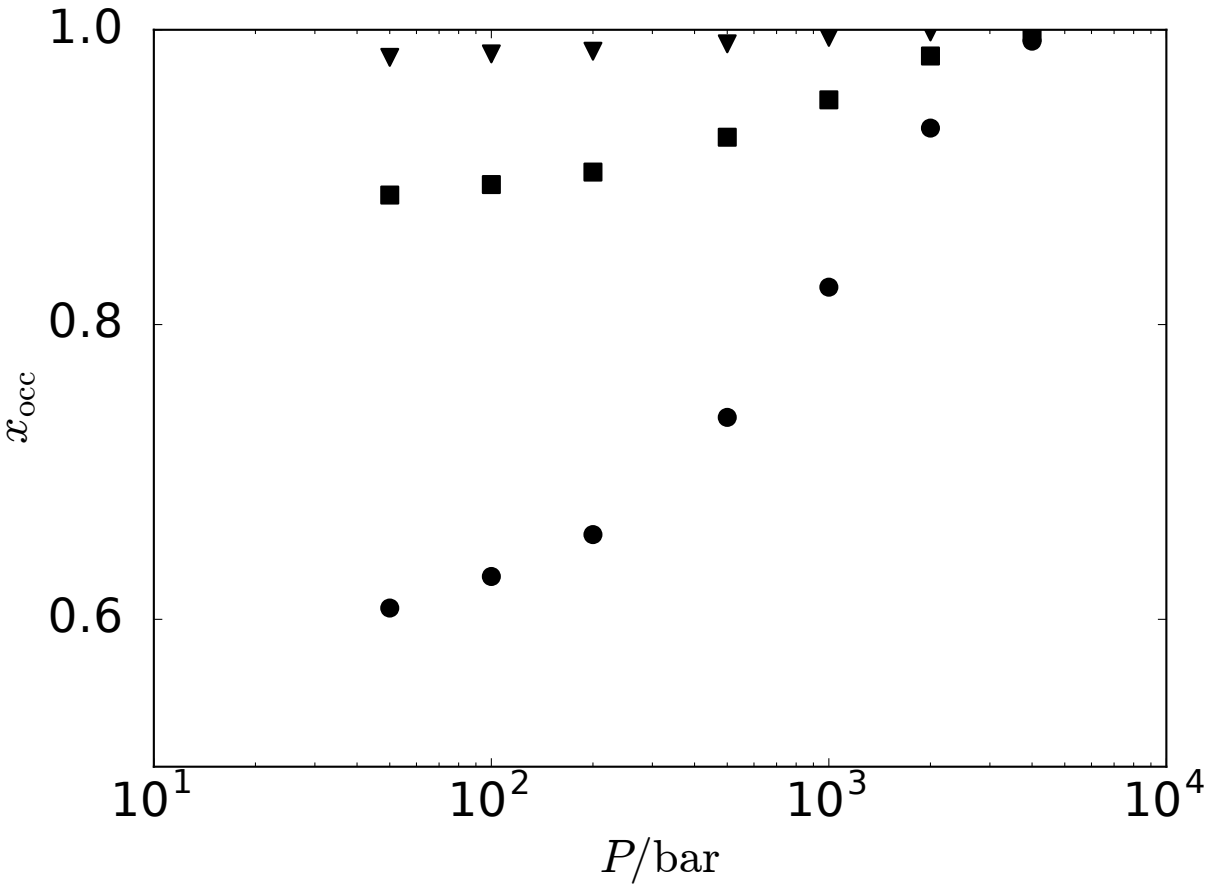


Figure 7: Fractional occupancy $x_{\mathrm{occ}}$ of TraPPE carbon dioxide[40] in sI hydrate (simulated using the TIP4P/Ice[23] water model), as a function of pressure $f$, at the dissociation temperature. Triangles represent the fractional occupancy of the large cages, circles the small cages, while squares represent the total fractional occupancy.

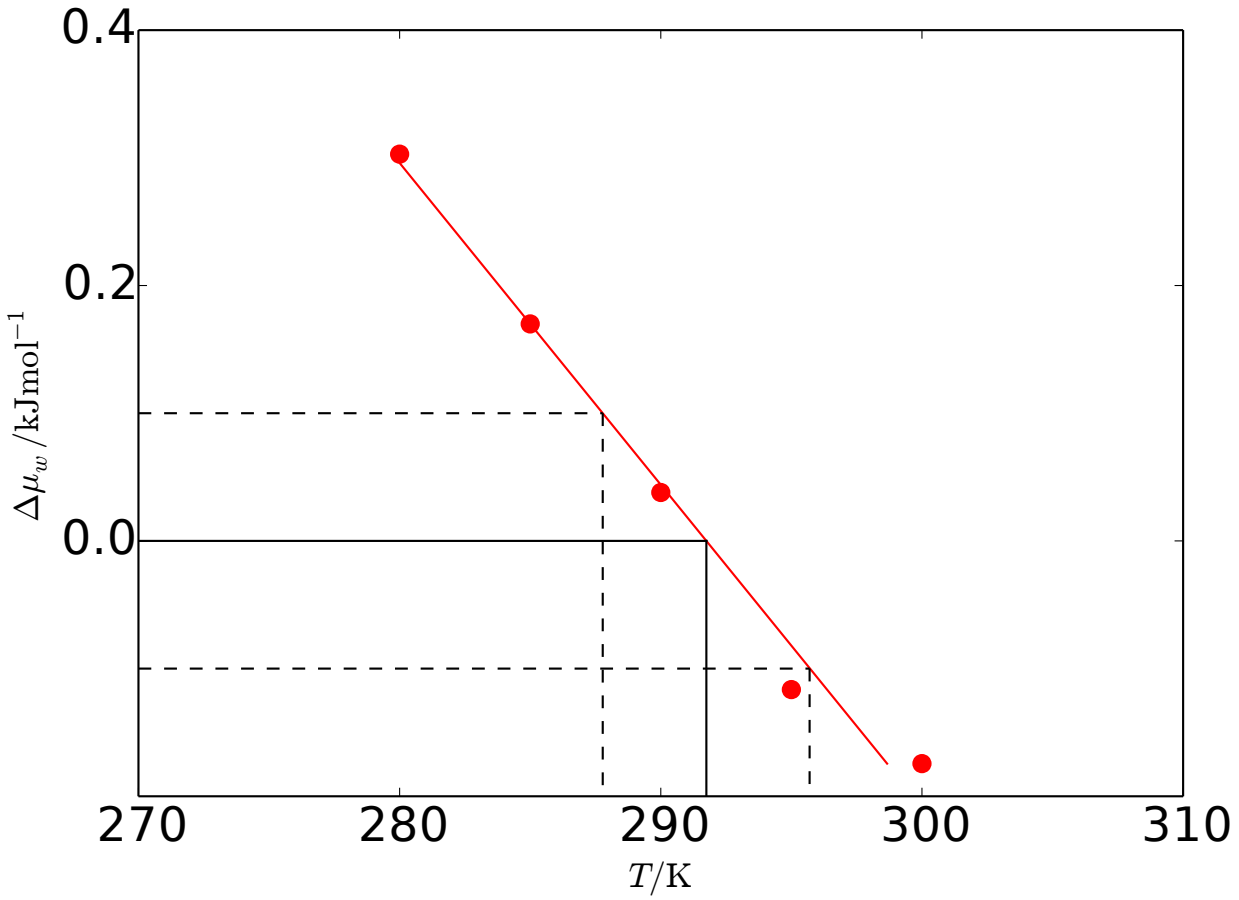


Figure 8: Temperature $T$, as a function of difference in water chemical potential, $\Delta\mu_{\mathrm{w}}$ between liquid water and TIP4P/Ice[23] hydrate filled with OPLS-UA methane[24], evaluated at a pressure of 200 bar. The slope represents a linear fit to the simulation results. The intercept of the linear fit is the three-phase equilibrium point.

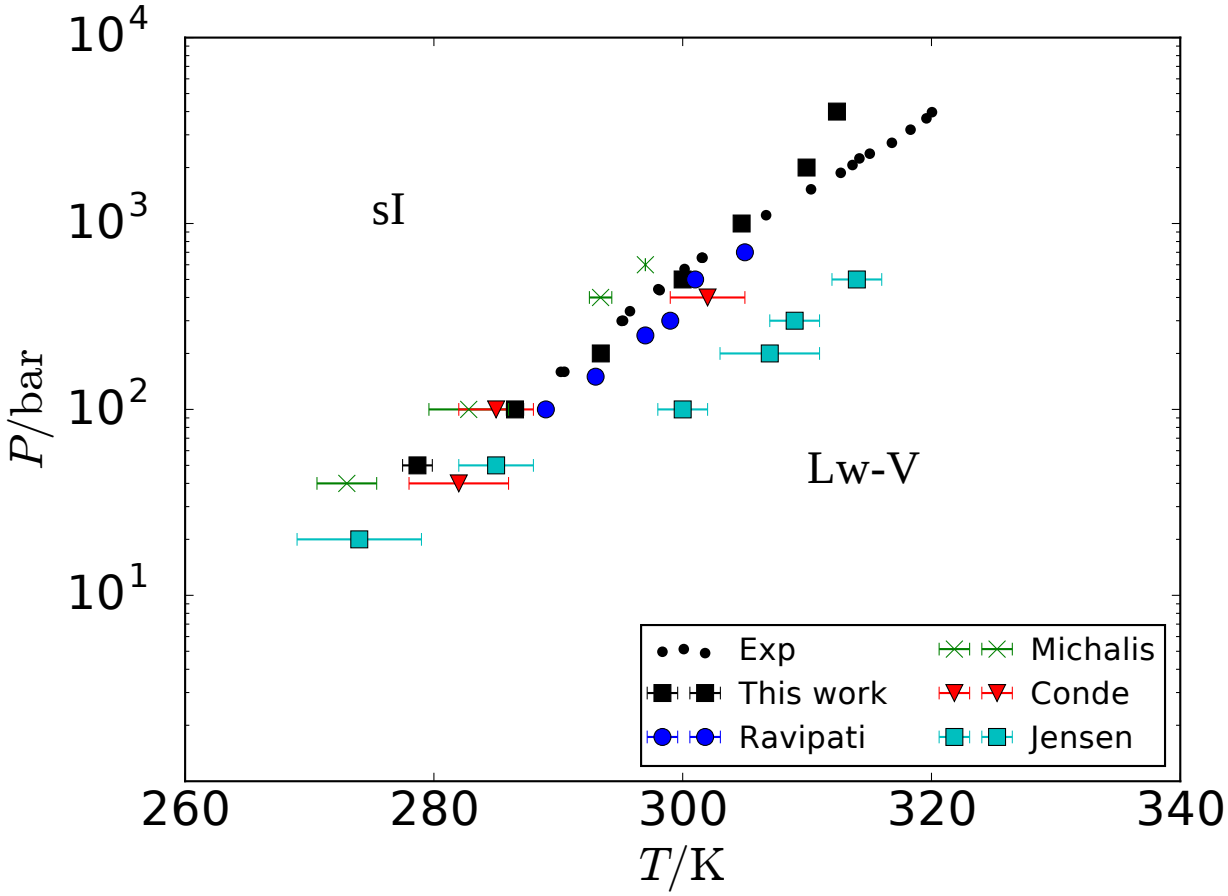


Figure 9: Three phase equilibrium points between sI hydrate (sI), liquid water (Lw) and gas vapor (V) for OPLS-UA methane[24] and TIP4P/Ice[23] hydrate. Experimental data from Marshall et al.[2]. Simulations due to Monte Carlo simulations from from Jensen et al.[22] and Ravipati and Punnathanam[26]. Direct coexistence simulations from Michalis et al.[16] and from Conde and Vega[15]

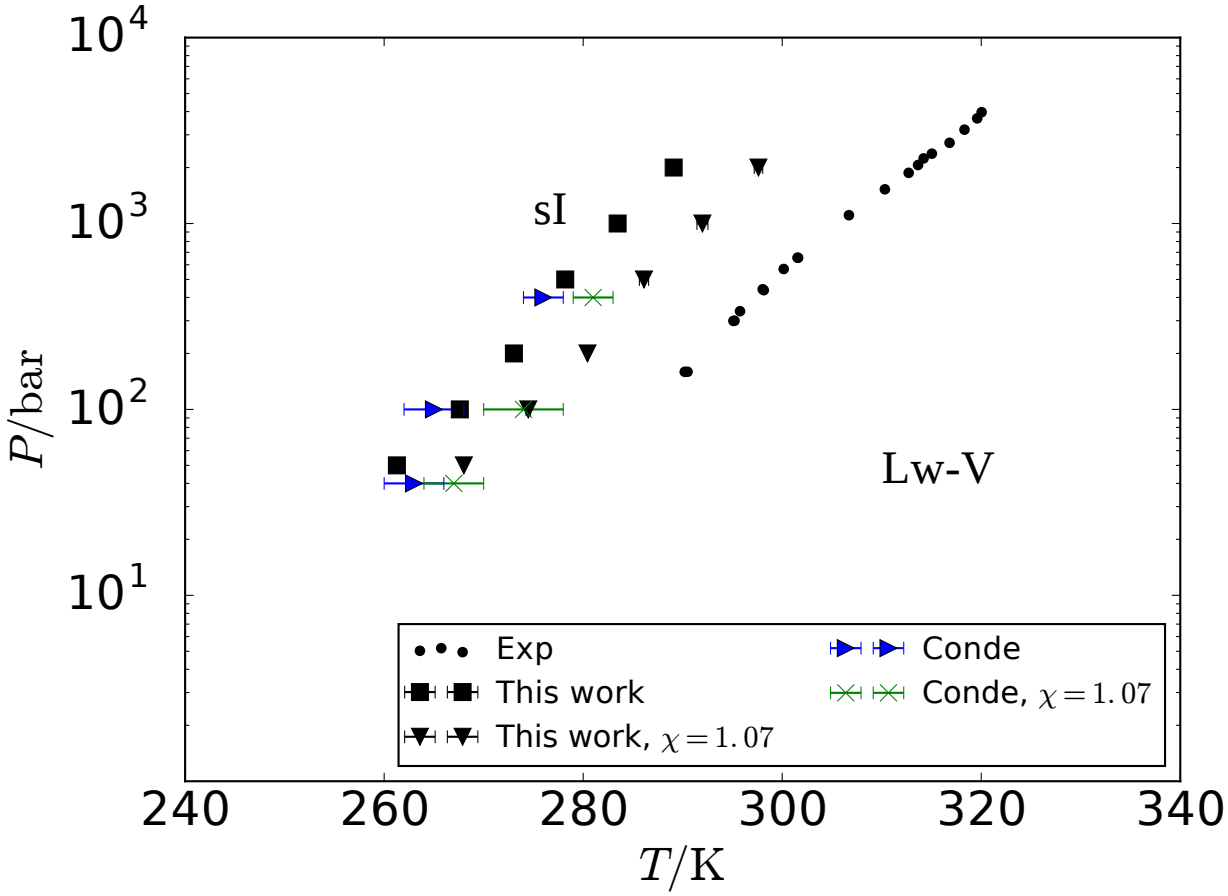


Figure 10: Three phase equilibrium points between sI hydrate (sI), liquid water (Lw) and gas vapor (V) for OPLS-UA methane[24] and TIP4P/2005[39] hydrate. Experimental data from Marshall et al.[2]. Direct coexistence simulations from Conde and Vega[15].

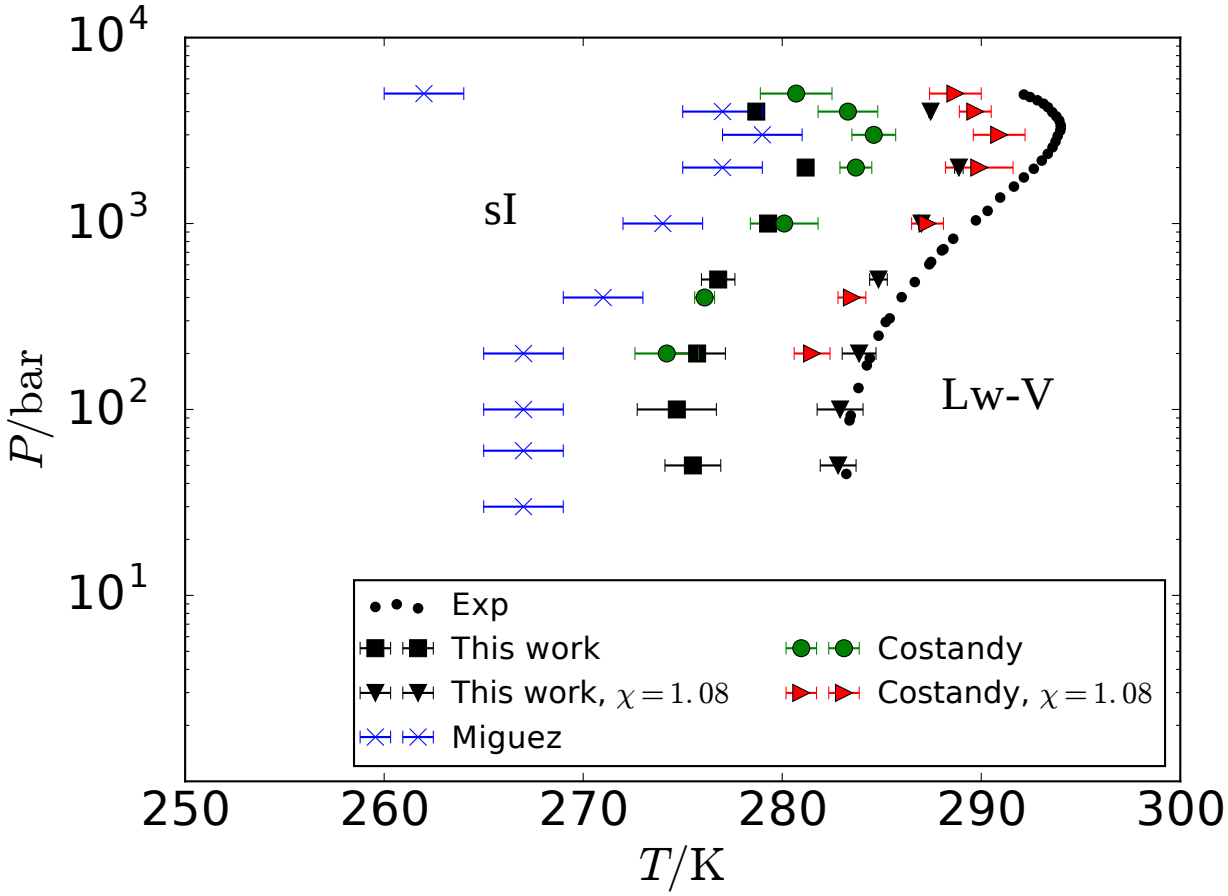


Figure 11: Three phase equilibrium points between sI hydrate (sI), liquid water (Lw) and gas vapor (V) for $CO_2$ hydrate, simulated using TraPPE $CO_2$[40] and TIP4P/Ice[23], together with experimental results[3,4], and direct coexistence simulations from Costandy et al.[18] and Miguez et al.[17]

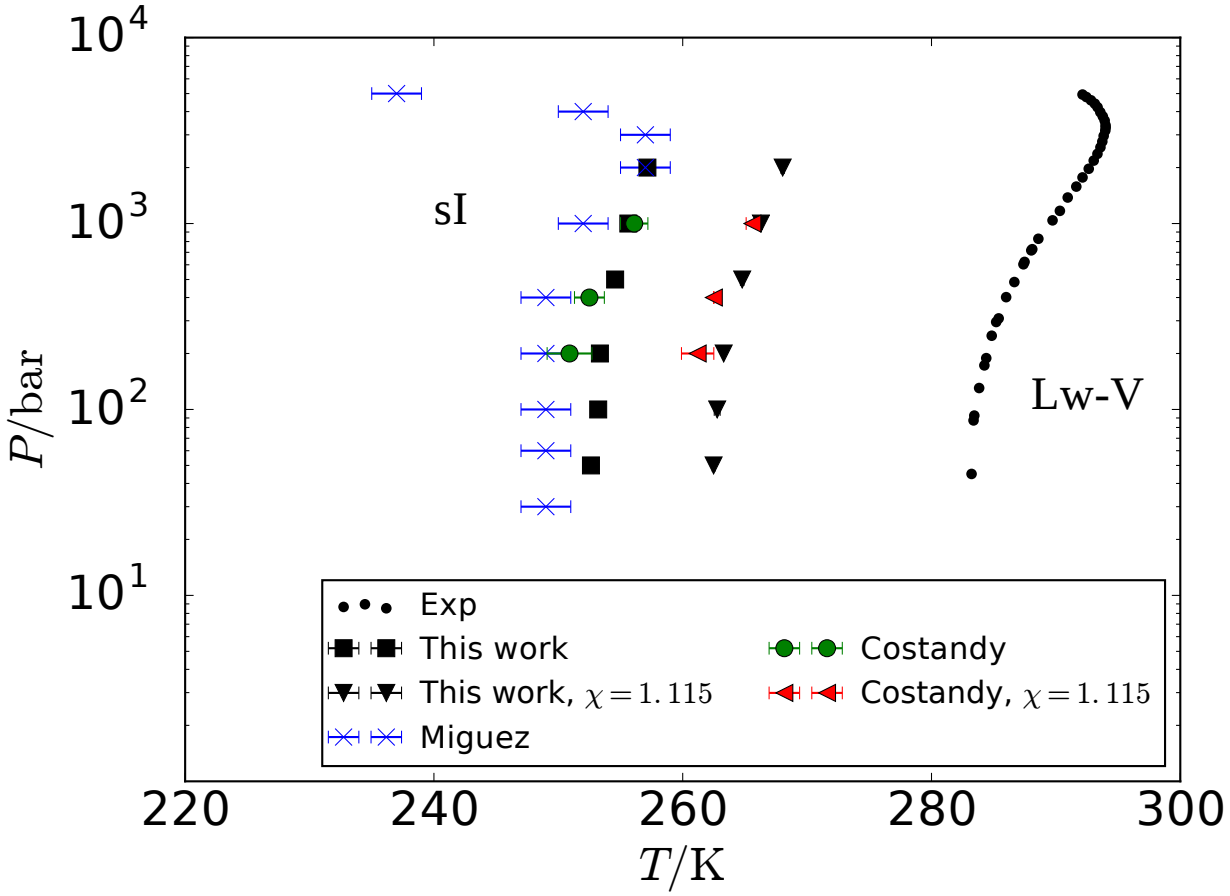


Figure 12: Three phase equilibrium points between sI hydrate (sI), liquid water (Lw) and gas vapor (V) for $CO_2$ hydrate, simulated using TraPPE $CO_2$[40] and TIP4P/2005[39] water, together with experimental results[3,4], and direct coexistence simulations from Costandy et al.[18] and Miguez et al.[17]

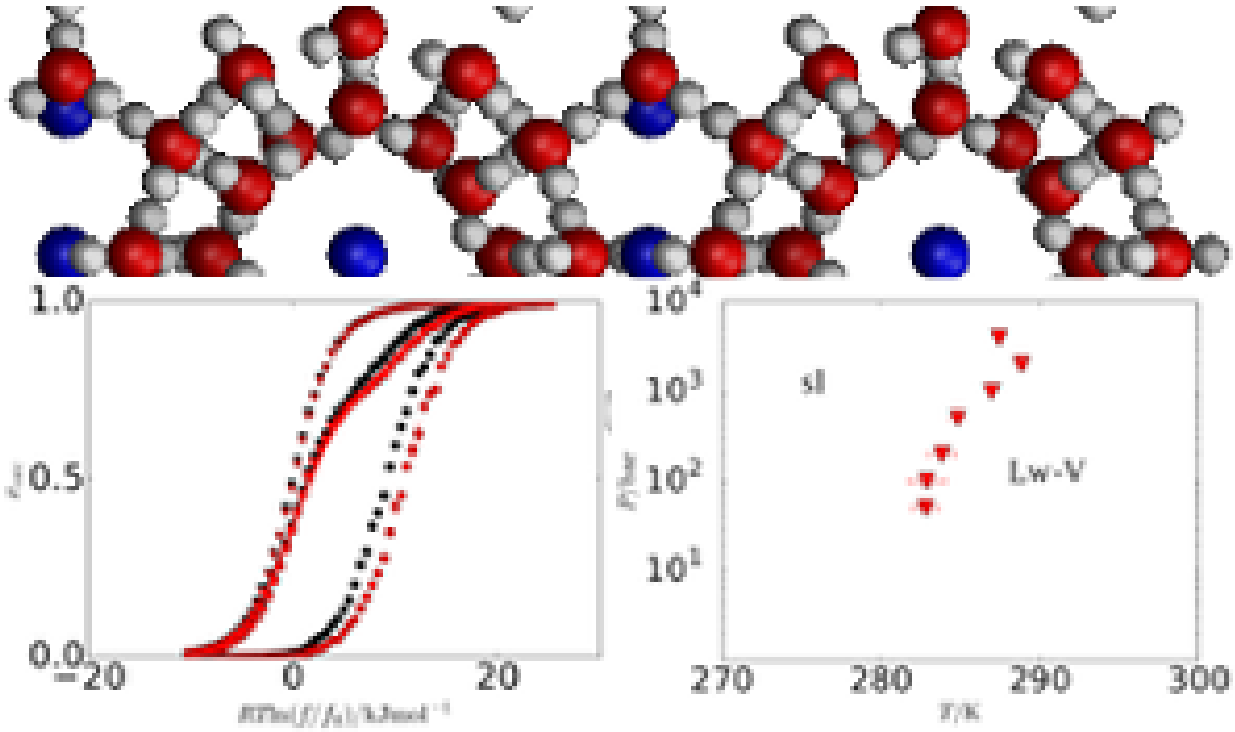
1.0
0.5
0.0
−20
0
20
sI
Lw-V
$10^4$
$10^3$
$10^2$
$10^1$
270
280
290
300
T/K